Chapter 6
Positive Position Feedback (PPF) Control

Abstract This chapter presents the design of a positive position feedback (PPF) controller based on low-pass filters and band-pass filters. In Sect. 6.1, the principle of the PPF controller is presented based on the single degree of freedom (SDOF) case. In Sect. 6.2, the loudspeaker–duct model is developed, several model interconnection methods in MATLAB are presented, and then the influence of loudspeaker dynamics is discussed. In Sect. 6.3, for the loudspeaker/microphone pair at the same location, the design of a PPF controller with an all-pass filter as phase compensation is presented. The Nyquist diagram, gain and phase margin, and root locus analysis are used to analyze the stability of the PPF controller. In Sect. 6.4, the PPF controller is extended for non-collocated loudspeaker/microphone pair. The calculation results show that the similar sound pressure reduction can be obtained by using a PPF controller with a non-collocated loudspeaker/microphone pair. In Sect. 6.5, the multimode control is discussed by using a single loudspeaker/microphone pair. In Sect. 6.6, a GUI program is given to design and analyze the PPF controller for a loudspeaker–duct model. And then we discuss how to share data between Simulink and GUI programs. In Sect. 6.7, the analog circuit for design of PPF controllers and all-pass filters are presented. Finally, some experimental results are presented to verify the simulation results.

6.1 Conception of PPF Controller

6.1.1 Active Damping with Collocated Pairs (Velocity Feedback and Resonant Controller)

For a slight damping structure with a collocated actuator/sensor pair, the transfer function has an alternating pole/zero pattern slightly to the left side of the imaginary axis. This property is very important, because several active damping approaches can be used with guaranteed stability. There we present several active damping approaches.

Q. Mao and S. Pietrzko, *Control of Noise and Structural Vibration: A MATLAB®-Based Approach*, DOI 10.1007/978-1-4471-5091-6_6, © Springer-Verlag London 2013

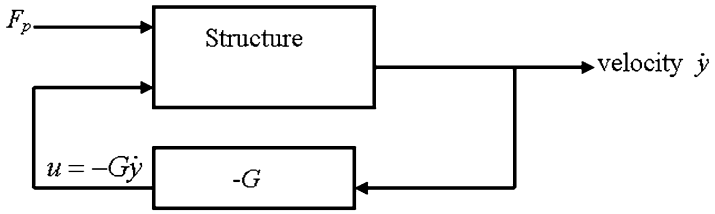

Fig. 6.1 Direct velocity feedback control

Firstly, we discuss the single-input–single-output (SISO) direct velocity feedback control system, as shown in Fig. 6.1. Assume that $\dot{y}$ is the measured velocity, and u is the collocated control force. The damping can be added by negative proportional feedback on $\dot{y}$ (direct velocity feedback). The governing equations are

$$M_s\ddot{x} + C_s\dot{x} + K_s x = F_p + Bu \tag{6.1a}$$

$$\dot{y} = B^{\mathrm{T}}\dot{x} \tag{6.1b}$$

$$u = -G\dot{y} \tag{6.1c}$$

where x is the displacement of the system. F_p and Bu are the primary and control modal force, respectively. M_s, C_s, and K_s are the mass, damping, and stiffness matrix, respectively.

Substituting Eqs. (6.1b) and (6.1c) into Eq. (6.1a), one gets

$$M_s\ddot{x} + (C_s + BGB^{\mathrm{T}})\,\dot{x} + K_s x = F_p \tag{6.2}$$

Clearly $BGB^{\mathrm{T}} = GBB^{\mathrm{T}} \geq 0$, $\forall G > 0$. It can be found that the control force appears as a viscous damping. The velocity feedback controller ($G > 0$) can guarantee unconditional closed-loop stability for a collocated system [1]. Figure 6.2 shows the root locus plot of velocity feedback for the SDOF system.

Next, we present a controller involving acceleration feedback termed as a resonant controller, as shown in Fig. 6.3, which can be written as

$$K = \frac{Gs^2}{s^2 + 2\zeta_f\omega_f s + \omega_f^2} \tag{6.3}$$

where G is the gain of controller.

Notice that the input of the controller is the displacement; s^2 in Eq. (6.3) represents the acceleration dynamics. The purpose of the controller is to add damping to structure and reduce the vibration levels. This is done by shifting closed-loop poles of the system deeper into the left side of the complex pole/zero plane. The closed loop is always stable for $G > 0$. Typical root locus plots for single degree of freedom systems are shown in Fig. 6.4.

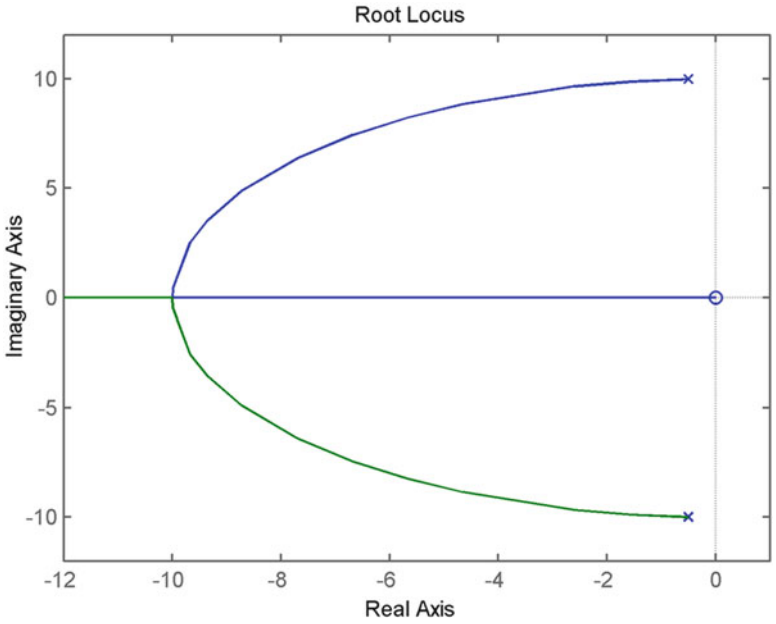

Fig. 6.2 The root locus plot of velocity feedback for SDOF system

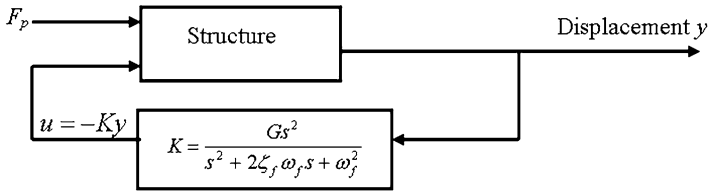

Fig. 6.3 Resonant feedback control

6.1.2 PPF Controllers (The Single Degree of Freedom Case)

The main difficulty in the implementation of velocity feedback and resonant feedback controllers is that the frequency responses of the controllers (in Eqs. (6.1c) and (6.3)) do not roll off at higher frequencies [2]. The closed-loop stability can be guaranteed when the collocated sensor/actuator pair is assumed to be perfect. However, for real applications, due to issues such as phase contributions of the sensor/actuator and uncertainty at high frequencies, the existence of out-of-bandwidth dynamics may destabilize the closed-loop system. To overcome this difficulty, we introduce the positive position feedback (PPF) controller to improve the roll-off of the control system, allowing high frequency gain stabilization.

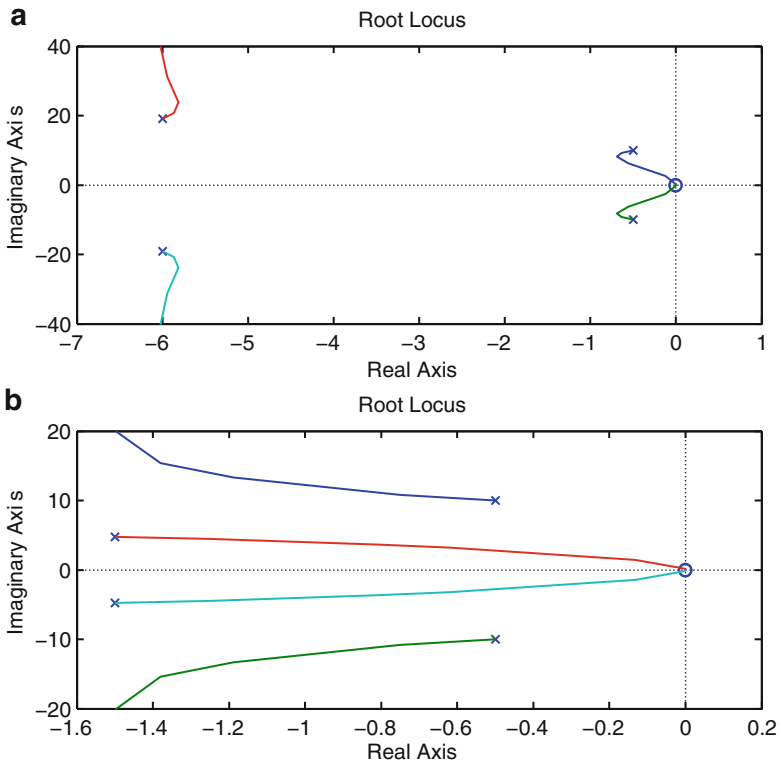

Fig. 6.4 The root locus plots of resonant control for single degree of freedom systems. (**a**) Controller resonance frequency $\omega_f >$ structural resonance frequency ω_s; (**b**) controller resonance frequency $\omega_f \leq$ structural resonance frequency ω_s

When the disturbance causing the structure to vibrate is random, the vibration is highly amplified at the resonant frequencies of the structure. Since not all the modes of vibration couple well with the acoustic plant, through which the radiated noise is propagating, the highly accentuated vibration at every mode of vibration does not necessarily result in severely radiated noise at the corresponding modes. In fact, vibration control for the sake of radiated noise reduction should be targeted at the structural modes with good coupling with the acoustic field. From this point, vibration damping at selectively chosen modes of a structure would be very effective in reducing the structure-borne noise. Feedback control using a positive position feedback (PPF) controller will accomplish the addition of damping to selective modes.

PPF controllers are basically a special form of second-order compensators [3–12]. The technique of PPF control was first introduced by Fanson and Caughey [3]. Its simplicity and robustness in experimental implementation has led to many applications in structural vibration control. Unlike other control laws, PPF is insensitive to the rather uncertain natural damping ratios of the structure.

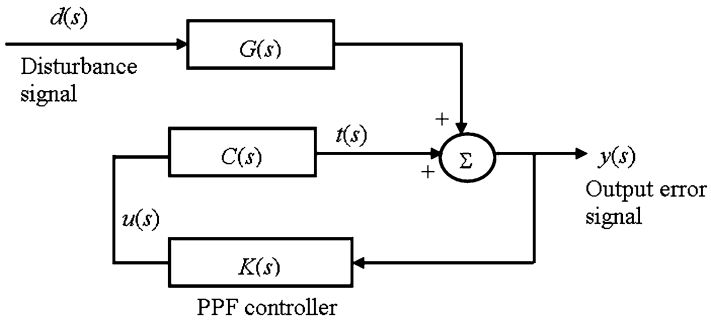

Fig. 6.5 Block diagram of PPF controller

A PPF controller includes a second-order low-pass filter, which can be tuned to resonate at the natural frequency of a structure, as illustrated in Fig. 6.1. In this Figure, $d(s)$ is the disturbance input and $y(s)$ is the displacement of the structure. $C(s)$ is the transfer function between the control force $u(t)$ and sensor. $G(s)$ is the transfer function between the disturbance input $d(s)$ and sensor, which is difficult to determine in practice.

The PPF controller in Fig. 6.5 is a highly damped (damping ratio of around 20–40 %) second-order low-pass filter that is tuned to the resonance frequency of the structure, similar to a tuned mass damper. For a collocated sensor/actuator configuration, both the structure $G(s)$ and low-pass filter each provide $-90°$ of phase shift at the resonance frequency. Since the phase of the controller is added in series, the response of the structure and PPF controller together provides 180° of phase at the resonance frequency. This signal $t(s)$ is then positively fed back to the disturbance signal $d(s)$, which results in more damping in the feedback-controlled structure. The advantage of the PPF controller is that it does not need any sensory information on the excitation source. Moreover, due to the simplicity of its structure, the PPF controller can readily be implemented using a low-cost analog circuit. The terminology *positive position* is derived from the fact that the position measurement is *positively* fed into the compensator and the position signal from the compensator is positively fed back to the structure. This property makes the PPF controller very suitable for collocated actuator/sensor pairs.

Assume a single degree of freedom structure is controlled by a single-input–single-output (SISO) system, as shown in Fig. 6.6. The dynamics of SDOF systems can be described in the following second-order differential equation:

$$M_s\ddot{x} + C_s\dot{x} + K_s x = F_p + q \tag{6.4}$$

where x is the displacement of the SDOF system. F_p and q are the primary and control force, respectively. M_s, C_s, and K_s are the mass, damping, and stiffness, respectively. $M_s = 1$, $C_s = 1$, and $K_s = 100$ are used in this study.

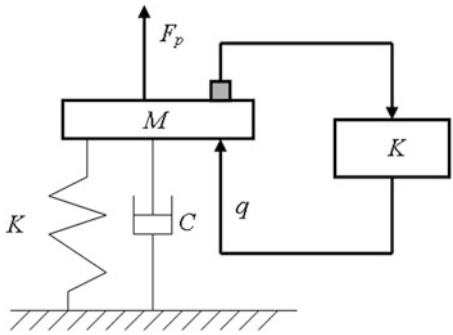

Fig. 6.6 A SDOF system with PPF controller K

The frequency response function of the positive position feedback (PPF) controller K is

$$\ddot{q} + 2\zeta_f \omega_f \dot{q} + \omega_f^2 q = g\omega_f^2 x \tag{6.5}$$

where ζ_f and ω_f are the damping ratio and natural frequency of the controller and g is a positive constant, termed scalar gain.

From Eq. (6.5), it can be found that there are three parameters ω_f, ζ_f, and g for the design of the PPF controller. Generally speaking, ω_f is set to be the same as the natural frequency of the structure ω_s, such as $\omega_f = \omega_s$. Figures 6.7 and 6.8 show the frequency response of the SDOF system and PPF controller when $\zeta_f = 0.3$ and $g = 20$. It can be found that the control path has $-180°$ phase shift at natural frequency $\omega_f = \omega_s = 10$ rad/s. Ten decibels (10 dB) velocity reduction can be observed around the natural frequency in Fig. 6.8.

Another two important parameters of PPF controllers are the damping ratio ζ_f and gain g. Figure 6.9 shows the effect of the damping ratio and gain of the PPF controller. If the damping is too high, the controller becomes uncoupled with the structural vibration and no longer dissipates energy effectively. Alternatively, if smaller damping effects are added, the two new modes are both fairly lightly damped. This results in very effective narrow-band absorption. However, broadband attention is desired in most applications. The larger the gain g of the controller, the further apart the two new resonances of the closed-loop system will be. By adding damping to the controller, both new resonances are well damped and significant broadband attenuation can be achieved. The value of ζ_f is typically selected between 0.2 and 0.4. It is important to note that the PPF controller is not unconditional stable. Figure 6.10 shows the Nyquist diagram with different gains. If the gain g is too large, for example, $g = 200$, the system will be unstable.

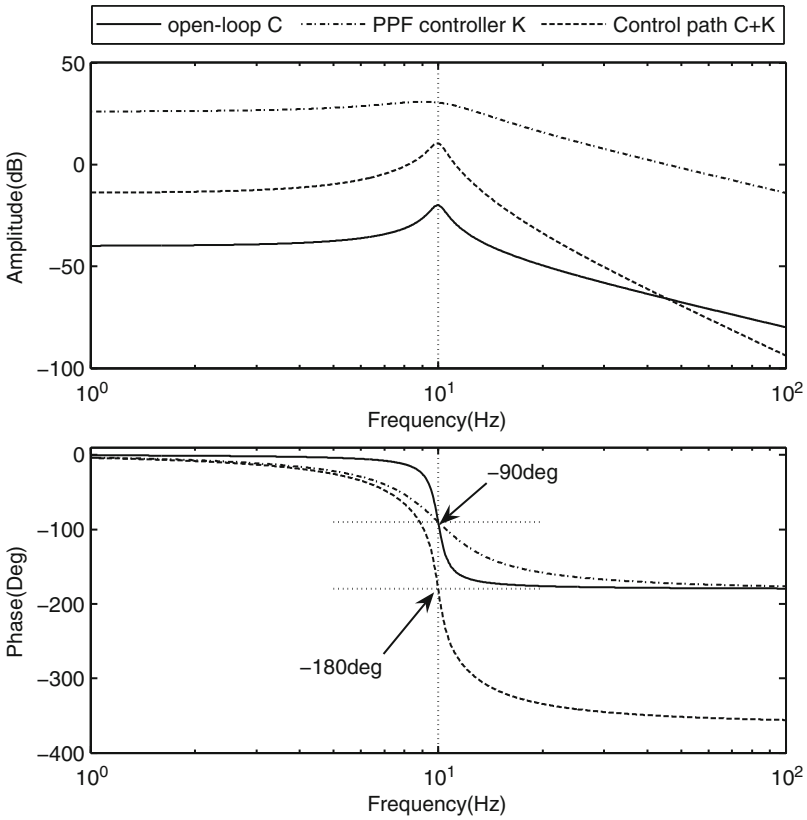

Fig. 6.7 Frequency response of a SDOF system and PPF controller

6.2 Control of the Sound Pressure in Duct by Using a PPF Controller

In this section, we discuss the control of sound pressure in a rigid-wall duct by using a PPF controller. The conception of the PPF controller will be extended for non-collocated actuator/sensor pair. Since the control actuator is a loudspeaker, which adds the additional unwanted phase to control path, an all-pass filter is used to compensate the phase shift due to loudspeaker dynamics. Furthermore, to realize the multimode control, the band-pass filters, rather than low-pass filters, will be used as a PPF controller. The roll-off associated with band-pass filters can limit interactions between adjacent modes.

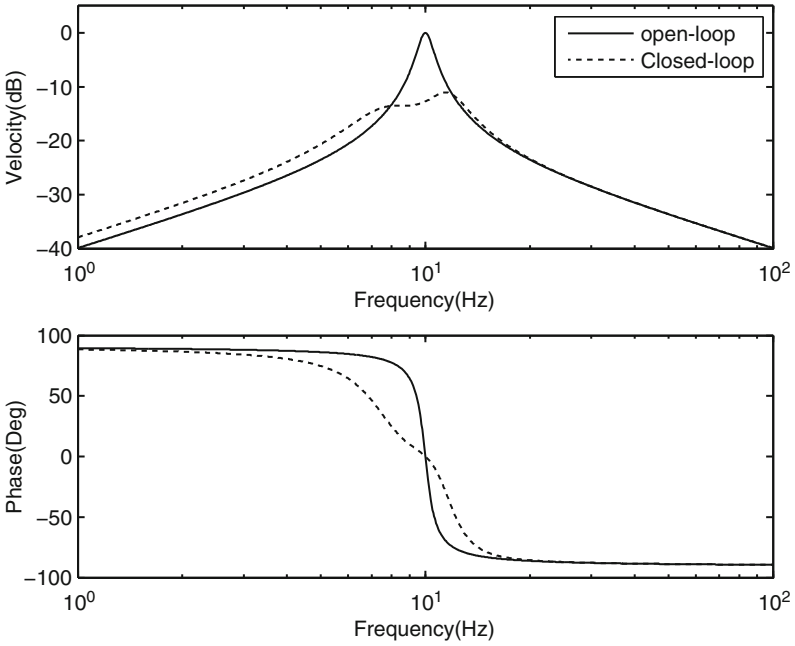

Fig. 6.8 Frequency response of the open loop and closed loop

6.2.1 Loudspeaker Model

A generic schematic for a cone loudspeaker is presented in Fig. 6.11. There are two inputs for the loudspeaker including the pressure acting on the speaker face and the voltage to the coil. The output is the volume velocity of the speaker, which acoustically excites the duct. Since loudspeakers are coupled electromechanical systems, two differential equations are needed to describe their behavior.

The motion of the loudspeaker cone can be written as [13]

$$M_m\ddot{x} + R_m\dot{x} + K_m x = Bl \cdot I - pA \tag{6.6}$$

$$p = p_F - p_R \tag{6.7}$$

$$p_R = -\frac{A\rho_0 c_0^2}{V_s}x \tag{6.8}$$

where M_m, K_m, and R_m are moving mass, stiffness, and damping of loudspeaker, respectively. x is the cone displacement. Bl is the force factor. I is the input current.

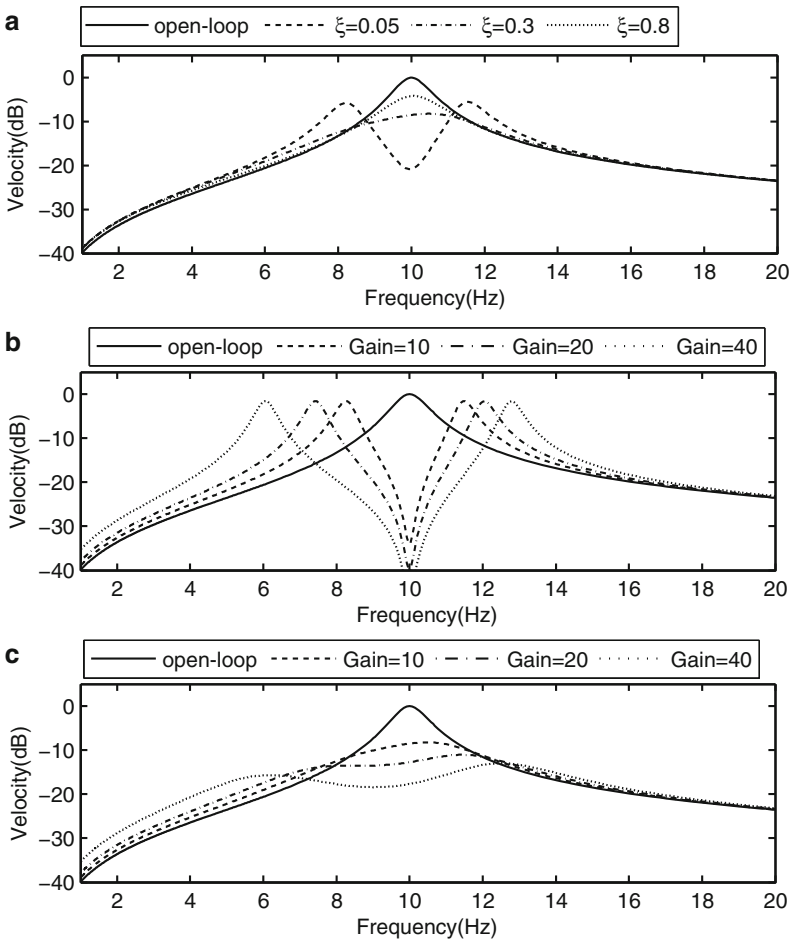

Fig. 6.9 The effect of the damping ratio and gain of the PPF controller. (**a**) Gain $g = 10$; (**b**) damping ratio $\zeta_f = 0.01$; (**c**) damping ratio $\zeta_f = 0.3$

Substituting Eqs.(6.7) and (6.8) into Eq. (6.6), we get

$$M_m\ddot{x} + R_m\dot{x} + \left(K_m + \frac{A^2\rho_0 c_0^2}{V_s}\right)x = Bl \cdot I - p_F A \tag{6.9}$$

And the electrical behavior of the loudspeaker can be written as [13]

$$L_m\dot{I} + R_m I = V_{\text{in}} - Bl \cdot \dot{x} \tag{6.10}$$

where L_m and R_m are the inductance and resistance of the loudspeaker. V_{in} is the input voltage applied to the coil.

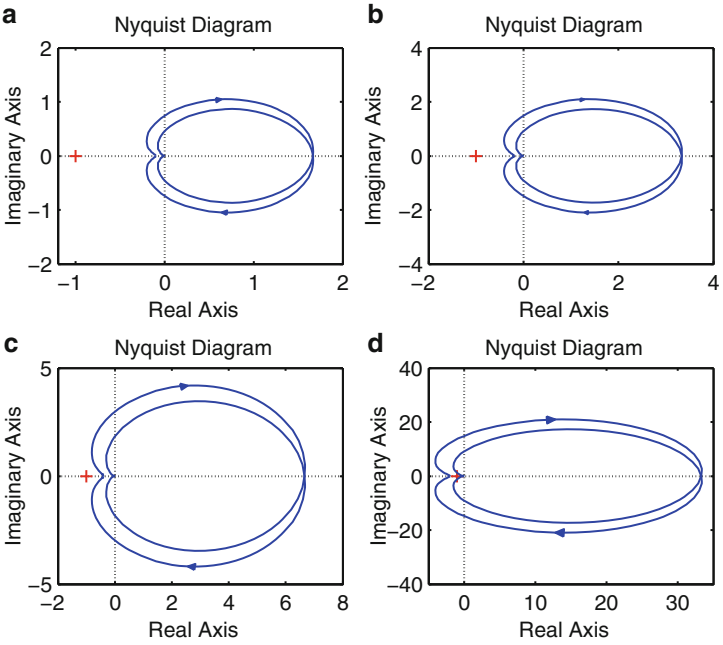

Fig. 6.10 Nyquist diagram with different gain of PPF controller when damping ratio $\zeta_f = 0.3$. (**a**) $g = 10$; (**b**) $g = 20$; (**c**) $g = 40$; (**d**) $g = 200$

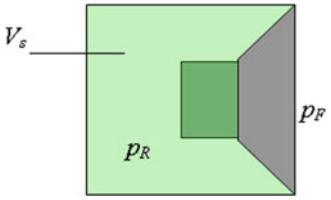

Fig. 6.11 The loudspeaker model

Equations (6.9) and (6.10) can be written in state-space model

$$\begin{bmatrix} \dot{I} \\ \dot{x} \\ \ddot{x} \end{bmatrix} = \begin{bmatrix} -\frac{R_m}{L_m} & 0 & -\frac{Bl}{L_m} \\ 0 & 0 & 1 \\ \frac{Bl}{M_m} & -\frac{K_m}{M_m} & -\frac{R_m}{M_m} \end{bmatrix} \begin{bmatrix} I \\ x \\ \dot{x} \end{bmatrix} + \begin{bmatrix} \frac{1}{L_m} & 0 \\ 0 & 0 \\ 0 & -\frac{A}{M_m} \end{bmatrix} \begin{bmatrix} V_{\text{in}} \\ p_F \end{bmatrix} \tag{6.11a}$$

Assume the output parameter of loudspeaker is acceleration $\ddot{x}$:

$$\ddot{x} = \begin{bmatrix} \frac{Bl}{M_m} & -\frac{K_m}{M_m} & -\frac{R_m}{M_m} \end{bmatrix} \begin{bmatrix} I \\ x \\ \dot{x} \end{bmatrix} + \begin{bmatrix} 0 & -\frac{A}{M_m} \end{bmatrix} \begin{bmatrix} V_{\text{in}} \\ p_F \end{bmatrix} \tag{6.11b}$$

Below we give the M-file **speaker.m**, which can be used to compute the speaker state-space model and to save it in the MATLAB variable [A, B, C, D].

```
%%%%%The parameters of the loudspeaker
ST=Lx*Ly;       % the area of duct section
wc_s=28*2*pi;  % the natural frequency of loudspeaker
Ss=207e-4;      % the eff. area of cone (m^2)
Vs=ST*0.1;      % the volume of the loudspeaker box
                  (estimate) (m^3)
Ls=0.75e-3;     % inductance of loudspeaker (L)
Bl=9.9;         % force factor of loudspeaker (Tm)
Rs=6.2;         % resistance of loudspeaker (Om)
Ms=37e-3;       % Eff. moving mass (Kg)
Ks=Ms*wc_s^2;  % Stiffness of loudspeaker
Rnn=10.;       % Damping of loudspeaker (Estimate)
%%%%%%%%%%%%%%%%%%%%%%%%%%%%%%%%%%%%%%%%%%%%%%%%
Ks=Ks+c0^2*lo0*Ss^2/Vs;

A0=[-Rs/Ls,      0,           -Bl/Ls
    0,           0,       1
    Bl/Ms,       -Ks/Ms,      -Rnn/Ms];

B0=[1/Ls 0; 0 0; 0 -Ss/Ms];

C0=[Bl/Ms -Ks/Ms -Rnn/Ms];

D0=[0 -Ss/Ms];
sys_spk=ss(A0, B0, C0, D0);
```

This produces an SS object ***sys_spk*** that stores the state-space A, B, C, D matrices.

6.2.2 Duct Model

Figure 6.12 shows the duct model. One primary loudspeaker is used as a disturbance, and another loudspeaker is used as an actuator. The parameters of the loudspeakers and duct are listed in Table 6.1.

Following the work by Fahy [13], the acoustic field can be represented by using the inhomogeneous wave equation:

$$\nabla^2 p - \frac{1}{c_o^2}\frac{\partial^2 p}{\partial t^2} = 0 \tag{6.12}$$

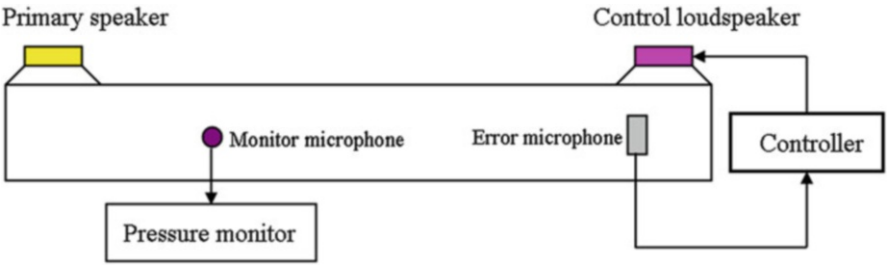

Fig. 6.12 The duct model

Table 6.1 The loudspeakers and duct parameters

Duct		Loudspeakers	
Parameter	Value	Parameter	Value
Length L_x (m)	4	Cone area S_S (m^2)	207×10^{-4}
Width L_y (m)	0.25	Moving mass M_S (kg)	37×10^{-3}
Height L_z (m)	0.25	Natural frequency ω_S (Hz)	28
Air density ρ_o (kg/m^2)	1.239	Speaker-box volume (m^3)	$S_s \times 0.1$
Sound speed c_o (m/s)	340	Force factor Bl (Tm)	9.9
		Inductance L_S (H)	0.37×10^{-3}
		Resistance R_S (ohms)	6.2

with boundary conditions

$$\frac{\partial p}{\partial \vec{n}} = \begin{cases} \rho_o \frac{\partial^2 w_p}{\partial t^2} & \text{on surface of primary loudspeaker} \\ \rho_o \frac{\partial^2 w_c}{\partial t^2} & \text{on surface of control loudspeaker} \\ 0 & \text{otherwise} \end{cases}$$

where ρ_o and c_o are the density and sound speed of the air, respectively. $\vec{n}$ is the positive inward normal component (normal to the loudspeaker vibrating surface). w_p and w_c are the displacement of primary and control loudspeakers, respectively.

For a rigid rectangular duct, we can use enclosure acoustic modes to compute the sound response. The pressure in enclosure can be represented in modal coordinates as

$$p(x, y, z) = \sum_n \Omega_n(x, y, z) P_n \tag{6.13}$$

with the property

$$\nabla^2 \Omega_n + \left(\frac{\omega_n}{c_o}\right)^2 \Omega_n = 0 \tag{6.14}$$

Table 6.2 The natural frequencies of the duct (Hz)

Index	1	2	3	4	5	6
Value	42.5	85.0	127.5	170.0	212.5	255.0
Index	7	8	9	10	11	12
Value	297.5	340.0	382.5	425.0	467.5	510.0

where P_n is the nth acoustic modal coordinate, and Ω_n is the nth acoustic mode shape of the rigid duct and has been normalized such that $\int_V \Omega_n^2(x, y, z)\mathrm{d}V = 1$.

For sufficiently low frequencies (below the cutoff frequency f_c), the acoustic response of the duct illustrated in Fig. 6.12 can be approximated by considering a one-dimension model. From Table 6.1, the cutoff frequency can be calculated by $f_c = \frac{\pi c_o}{L_y} = 4,273$ rad/s $= 680$ Hz; the first 12 modes (0–510 Hz), which are listed in Table 6.2, are used to establish the duct model.

In this study, we consider the control of the duct pressure below 300 Hz. Equation (6.13) can be simplified as

$$p(x) = \sum_n \Omega_n(x) P_n \tag{6.15}$$

where

$$\Omega_n(x) = \sqrt{\frac{2}{L_x}} \cos\left(\frac{n\pi x}{L_x}\right) \tag{6.16}$$

From Eq. (6.16), it is easy to find that

$$\int_0^{L_x} \Omega_n^2(x)\mathrm{d}x = 1 \tag{6.17}$$

Substituting Eq. (6.15) into Eq. (6.12) and applying orthogonality in Eq. (6.17), then taking into account the viscous damping terms, the final governing equation for the duct is as follows:

$$\ddot{P}_n + 2\zeta_n\omega_n\dot{P}_n + \omega_n^2 P_n = \rho_o c_o^2(F_{p,n} + F_{c,n}) \tag{6.18}$$

where ω_n and ζ_n are the nth natural frequency and damping ratio of the acoustic mode. $F_{p,n}$ and $F_{c,n}$ are the nth modal force due to primary loudspeaker and control loudspeaker, respectively.

$$F_{k,n} = \int_{S_{sp}} \ddot{w}_k \Omega_n(x)\mathrm{d}S_{sp} \quad (k = p \text{ or } c) \tag{6.19}$$

where S_{sp} is the area of cone of the speaker.

Since the cross-sectional area of the speaker S_{sp} is quite small, Eq. (6.19) can be rewritten as

$$F_{k,n} = \ddot{w}_k \Omega_n(x_k) S_{sp} \quad (k = p \text{ or } c) \tag{6.20}$$

where S_{sp} is the area of cone of the speaker and x_k is the loudspeaker location.

Assume there are two loudspeakers in duct, one is a primary and another is a control loudspeaker. Equation (6.18) can be written as a state-space model

$$\begin{bmatrix} \dot{P} \\ \ddot{P} \end{bmatrix} = \begin{bmatrix} 0_{N\times N} & I_{N\times N} \\ -(\omega^p)^2 & -2\zeta^p\omega^p \end{bmatrix} \begin{bmatrix} P \\ \dot{P} \end{bmatrix} + \begin{bmatrix} 0_{1\times N} & 0_{1\times N} \\ S_{sp}\Omega_p & S_{sp}\Omega_c \end{bmatrix} \begin{bmatrix} \ddot{x}_p \\ \ddot{x}_c \end{bmatrix} \tag{6.21a}$$

There are four output parameters, i.e., the pressure at the primary speaker location Ω_p, the pressure at the control speaker location Ω_c, the pressure at error microphone location $\Omega_{s,}$ and monitor microphone location Ω_m:

$$\begin{bmatrix} p_p \\ p_c \\ p_s \\ p_m \end{bmatrix} = \begin{bmatrix} \Omega_p & 0 \\ \Omega_c & 0 \\ \Omega_s & 0 \\ \Omega_m & 0 \end{bmatrix} \begin{bmatrix} P \\ \dot{P} \end{bmatrix} \tag{6.21b}$$

Below we give the M-file **duct.m**, which can be used to compute the duct state-space model and produces an SS object ***sys_duct***.

```
%%%%%%%%%%%%%% For duct model
EE=lo0*c0^2/(Lz*Lx*Ly);

AD=[zeros(Nmod,Nmod) eye(Nmod); -wr.^2 -2*nnnr*wr];

BD(:,1)=[zeros(Nmod, 1); EE * Ss * Paa.'];
BD(:,2)=[zeros(Nmod, 1); EE * Ss * Pcc.'];

CD=[Paa zeros(1, Nmod);   %% pressure at primary
                             loudspeaker
    Pmm zeros(1, Nmod)    %% pressure at error sensor
    Pss zeros(1, Nmod)    %% pressure at monitor
                             microphone
    Pcc zeros(1, Nmod)];  %% pressure at control
                             loudspeaker

DD = zeros(4,2);

sys_duct=ss(AD,BD,CD,DD);
```

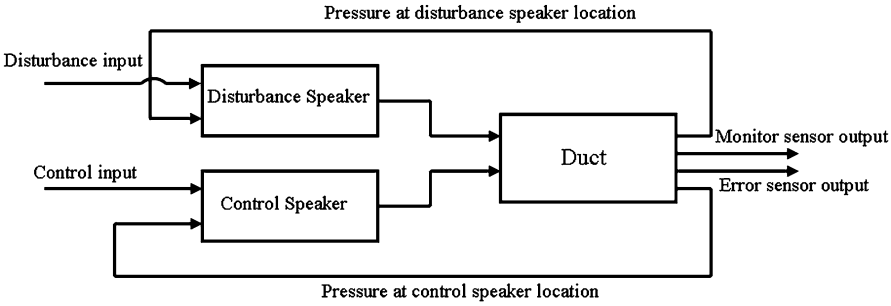

Fig. 6.13 The duct–loudspeaker system

Table 6.3 Interconnection functions

Interconnection functions	Description
append	To append models in block diagram configuration
connect	To work with command append to produce an arbitrary interconnection scheme to a set of models
lft	To form Redheffer star product (linear fractional transformation) of two models
feedback	To form the feedback interconnection of two models
parallel	To form parallel connection of two models
series	To form series connection of two models
sysic	To build an arbitrary interconnection scheme of systems
iconnect	An alternative to command sysic, and is used to build complex interconnections of systems
icsignal	To be used with command iconnect to specify signal constraints described by the interconnection of components

6.2.3 Loudspeaker–Duct Coupling Model

After we obtain the loudspeaker and duct models, the next step is to couple these models to establish a complete loudspeaker–duct model. Figure 6.13 shows the diagram of the loudspeaker–duct system interconnection. From Eqs. (6.21a) and (6.21b), it can be found that the accelerations of disturbance and control speaker are used as inputs of the duct model. There are four outputs of the duct model, i.e., pressure at disturbance speaker location which is pressure input of disturbance speaker, monitor sensor output to assess the control performance, error sensor output to drive the controller, and pressure at control speaker location which is pressure input of control speaker.

There are several interconnection methods in MATLAB. Control System Toolbox and Robust Control Toolbox support these interconnection functions which are summarized in Table 6.3.

Here we introduce three other methods to build the interconnection of systems:

1. By using command **sysic** which has been discussed in Chapter 5
2. By using commands **connect** and **append**
3. By using commands **iconnect** and **icsignal**

Below we give the M-file **ic_model.m**, which is used to compute the duct–loudspeaker state-space model by using different interconnection methods.

```
sysDT=sys_duct;
sysNS=sys_spk;
sysCS=sys_spk;
% Build the connection with loudspeaker and duct
  models
systemnames = ' sysDT sysNS sysCS';
inputvar = '[ dist; control]';
outputvar = '[sysDT(2:3)]';
input_to_sysDT = '[sysNS; sysCS]';
input_to_sysNS = '[dist; sysDT(1)]';
input_to_sysCS = '[control; sysDT(4)]';
sysoutname = 'sysUU';
cleanupsysic = 'yes';
sysic

dist      = icsignal(1);
control   = icsignal(1);
out       = icsignal(4);
yp        = icsignal(2);
MM        = iconnect;
MM.Input  = [dist; control];
MM.Output = [out(2:3)];
MM.Equation{1} = equate(out, sysDT*yp);
MM.Equation{2} = equate(yp,[sysNS*[dist; out(1)];
  sysCS*[control; out(4)]]);
sysUU=MM.system;
%%%%%%%%%%%%%
sysAA  = append(sysNS, sysCS, sysDT);
Q      = [2 3; 4 6; 5 1; 6 2];
inputs = [1 3];
outputs= [4 5];
sysUU  = connect(sysAA, Q, inputs, outputs);
```

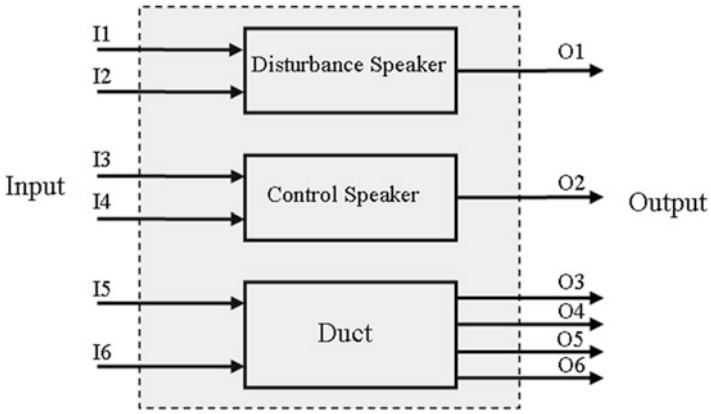

Fig. 6.14 The result of **append** function for the duct–loudspeaker system

Interconnection Model Using Functions append and connect

Starting with a block diagram description, we can use **append** and **connect** to construct a state-space model of the system.

First, use the command append with the following syntax:

```
sys = append(sys1,sys2,...,sysN)
```

to specify each block *sysj* in the diagram and form a block-diagonal, unconnected model sys of the diagram. The result of the append function produces a model which has a block diagram as shown in Fig. 6.10.

Next, use the following syntax:

```
sysc = connect(sys,Q,inputs,outputs)
```

to connect the blocks together and derive a state-space model **sysc** for the overall interconnection. The matrix Q indicates how the blocks on the diagram are connected. It has a row for each input of sys, where the first element of each row is the input number. The subsequent elements of each row specify where the block input gets its summing inputs; negative elements indicate minus inputs to the summing junction. The index vector's inputs and outputs indicate which of the inputs and outputs in the large unconnected system are external inputs and outputs of the block diagram.

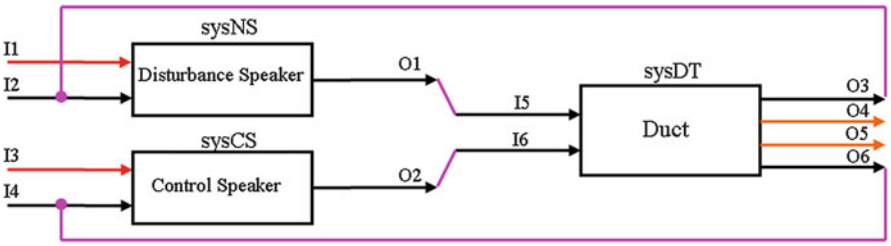

Fig. 6.15 The result of **connection** function for the duct–loudspeaker system

In this study, from Figs. 6.13 and 6.14, it can be found that the interconnection matrix Q = [2 3; 4 6; 5 1; 6 2] where I2, I4, I5, and I6 get signals from O3, O6, O1, and O2, respectively. Next, we can set inputs = [1 3] where I1 and I3 are the external inputs, and outputs = [4 5] where O4 and O5 are the external outputs. The interconnection model is presented in Fig. 6.15.

Interconnection Model Using Function sysic

The function **sysic** can be used to create an arbitrary interconnection model. The M-file below is used to create the interconnection shown in Fig. 6.15.

```
% Build the connection with loudspeaker and duct
  models
systemnames = ' sysDT sysNS sysCS';
inputvar = '[ dist; control]';
outputvar = '[sysDT(2:3)]';
input_to_sysDT = '[sysNS; sysCS]';
input_to_sysNS = '[dist; sysDT(1)]';
input_to_sysCS = '[control; sysDT(4)]';
sysoutname = 'sysUU';
cleanupsysic = 'yes';
sysic
```

Interconnection Model Using Functions iconnect and icsignal

The first step is to create four **icsignal** objects **dist** (I1 in Fig. 15), **control** (I3 in Fig. 6.15), **out** ([O3 O4 O5 O6] in Fig. 15), and **yp** ([O1 O2] in Fig. 6.15). Then create an empty **iconnection** object **MM**. From Figs. 6.13 and 6.15, it can be found that the loudspeaker–duct model has two inputs and two outputs. Now we define the input of the interconnection to be [dist; control], and the output to be [out(2:3)]. Then define two constraints among the **icsignal** object variables:

```
out = sysDT * yp, and yp = [sysNS * [dist out(1)];
sysCS * [control; out(4)]].
```

Below we give the M-file which is used to create an interconnection model using functions **iconnect** and **icsignal**. We can get the state-space model **sysUU** representation of the relationship between the input [dist; control] and the output [out(2:3)].

```
dist      = icsignal(1);
control   = icsignal(1);
out       = icsignal(4);
yp        = icsignal(2);
MM        = iconnect;
MM.Input  = [dist; control];
MM.Output = [out(2:3)];
MM.Equation{1} = equate(out, sysDT*yp);
MM.Equation{2} = equate(yp,[sysNS*[dist; out(1)];
sysCS*[control; out(4)]]);
sysUU=MM.system;
```

We can get the same results by using the three methods above to create the loudspeaker–duct model. For example, Figs. 6.16 and 6.17 show the FRFs of disturbance speaker to monitor microphone and control speaker to error microphone by using above the interconnection methods. It can be found that the FRFs are the same.

6.2.4 The Influence of Loudspeaker Dynamics

To demonstrate the influence of loudspeaker dynamics, the speaker–duct model is compared to the uncoupled model which is defined to be the loudspeaker replaced by an ideal volume velocity source. Assume that the control loudspeaker and error microphone are centered at the same location, such as $x_c = x_s = 3.88$ m. The Bode plots for the loudspeaker–duct model and volume velocity source–duct model are shown in Fig. 6.18. The amplitude response from each model is plotted separately, because the frequency response function (FRF) for the loudspeaker–duct model is expressed in units of pressure over input voltage, while the FRF for volume velocity–duct model is expressed in terms of pressure over input volume velocity. From Fig. 6.18, it can be found that the most significant difference between the FRFs of the two models is related to the phase. The phase response of the volume velocity–duct model varies between $\pm 90°$. However, the phase response of loudspeaker–duct model is significantly different with the collocated case (between $\pm 90°$) because of loudspeaker dynamics.

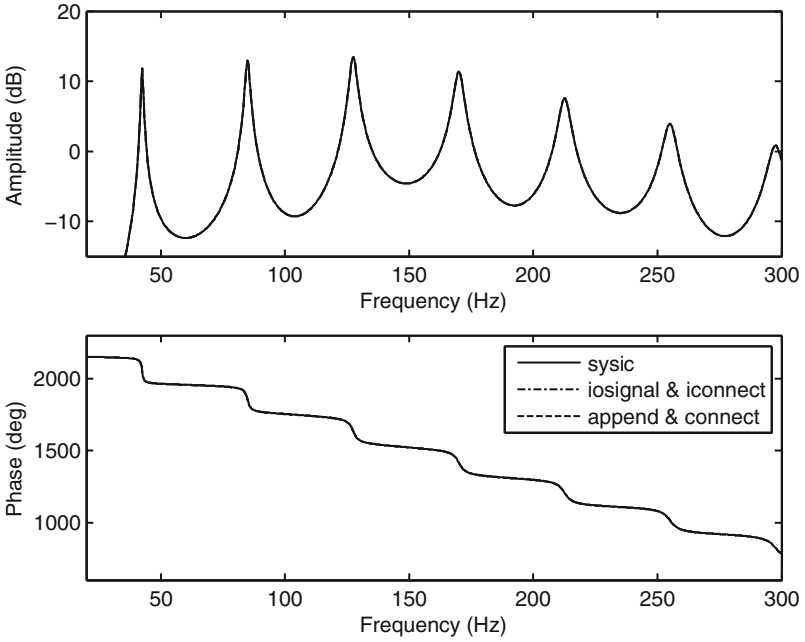

Fig. 6.16 The FRFs (disturbance speaker to monitor microphone) of loudspeaker–duct model which are created by using different methods

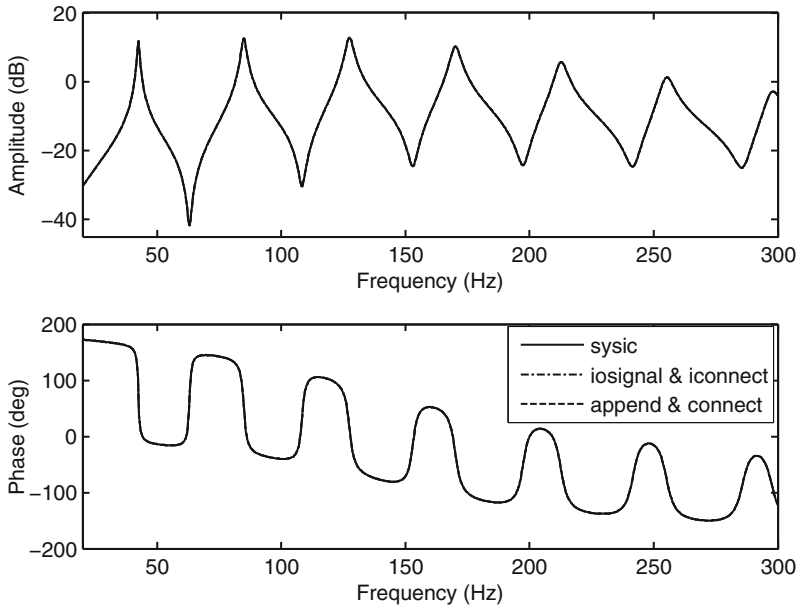

Fig. 6.17 The FRFs (control speaker to error microphone) of loudspeaker–duct model which are created by using different methods

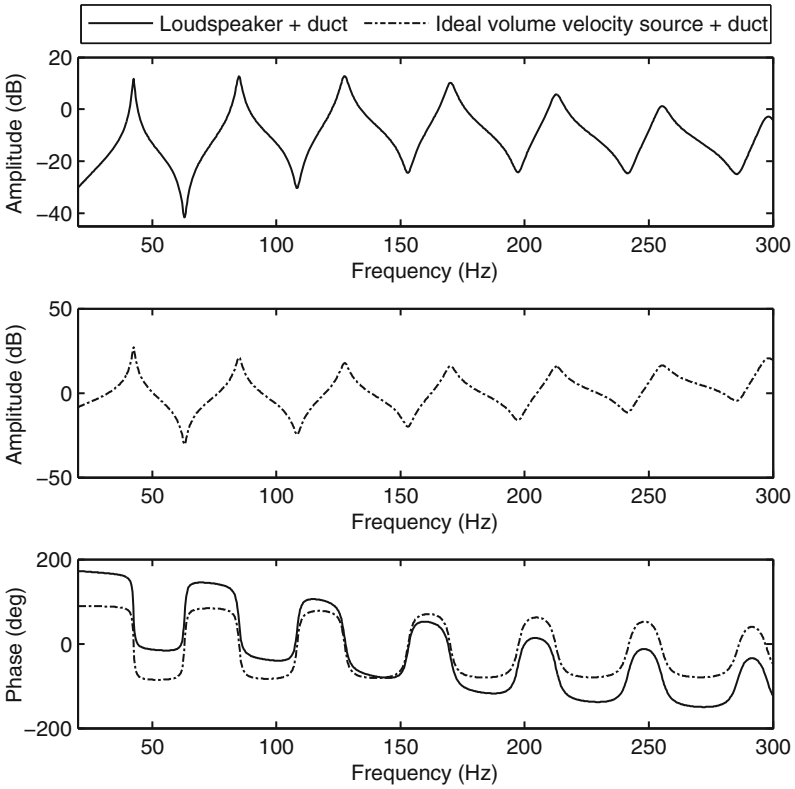

Fig. 6.18 Comparison of Bode plots for the speaker–duct coupling model and duct modelled with ideal volume velocity source

Figure 6.19 shows the FRFs of the duct and control loudspeaker. It can be found that the phase of the duct is always –90° at the resonance frequencies when input and output are collocated. When the loudspeaker is combined with the duct, the phase at resonance frequencies varies from 90° to –90°. To design a PPF controller, some form of phase compensation needs to be added to compensate the phase shift due to loudspeaker dynamics, so that the net phase response of control path at the control frequency is $\pm 180°$.

6.3 PPF Controller and Phase-Compensation Design

In this section, the design of a PPF controller is developed to control one or several duct modes. As to collocated structural PPF control as described in the above section, the collocated actuator/sensor and second-order low-pass filter are used to generate an output signal which has 180° phase shift with sensor signal at the

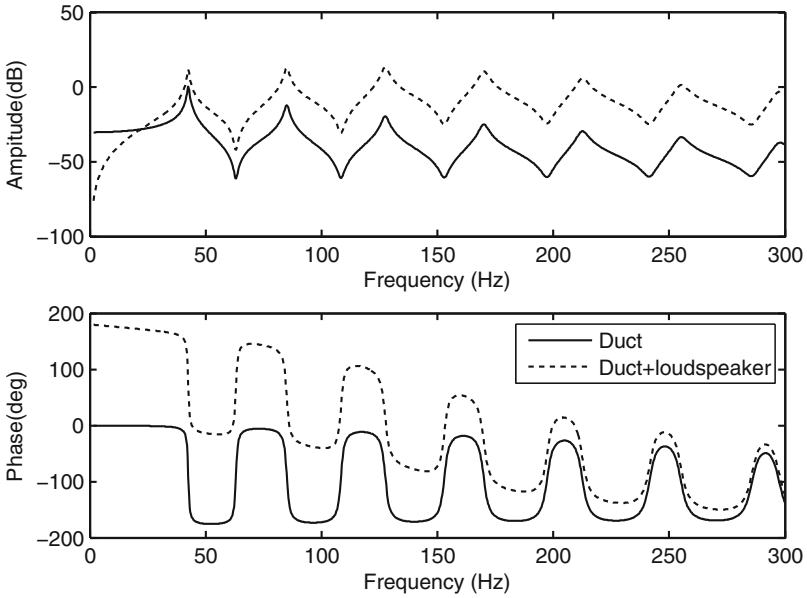

Fig. 6.19 The FRFs of the duct and control loudspeaker + duct

target control frequency. Unlike with collocated structural PPF control design, it is difficult to obtain a collocated loudspeaker/microphone pair due to loudspeaker dynamics, as described in Fig. 6.19. To obtain the required 180° phase shift at target frequency, a phase compensation should be used to compensate the phase of the control path.

Low-pass and band-pass second-order filters can be used as PPF controller and expressed as

$$H_{\mathrm{LP}}(s) = G\frac{\omega_{\mathrm{c}}^2}{s^2 + 2\zeta_{\mathrm{c}}\omega_{\mathrm{c}}s + \omega_{\mathrm{c}}^2} \tag{6.22}$$

$$H_{\mathrm{BP}}(s) = G\frac{\omega_{\mathrm{c}}s}{s^2 + 2\zeta_{\mathrm{c}}\omega_{\mathrm{c}}s + \omega_{\mathrm{c}}^2} \tag{6.23}$$

Figures 6.20 and 6.21 show the Bode plots of the low-pass and band-pass second-order filter responses. A low-pass filter provides fast roll-off of 40 dB/dec above ω_c, but yields little amplitude change below ω_c. In contrast, the band-pass filter provides roll-off of 20 dB/dec in both the low and high frequency ranges to either side of ω_c. However, the low-pass filter has a $-90°$ phase shift at the target frequency, and the band-pass filter has no phase shift (0°) at the target frequency.

The low-pass filter as PPF controller has been shown to work well for single or multimode control. However, the multimode control by using low-pass filters as a PPF controller may pose some problems due to the overlapping phases, since the

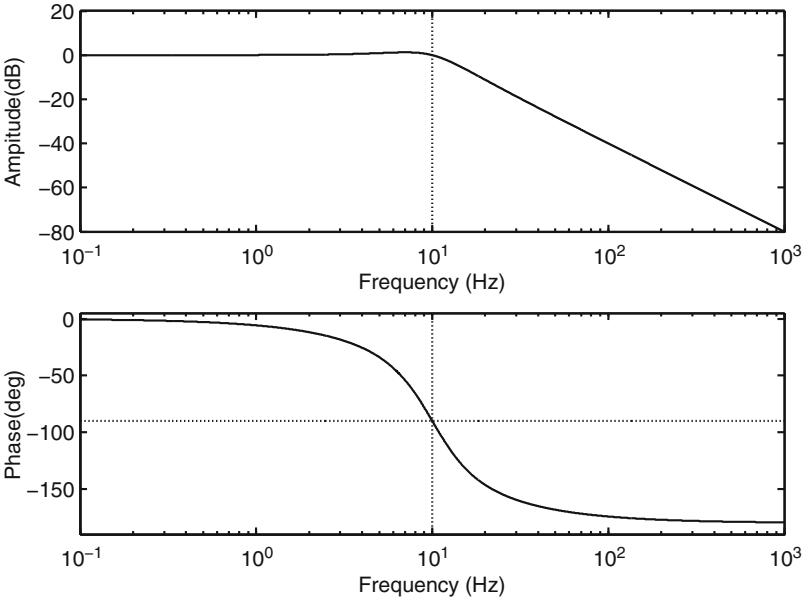

Fig. 6.20 Frequency response of the second low-pass filter when the gain $G = 1$

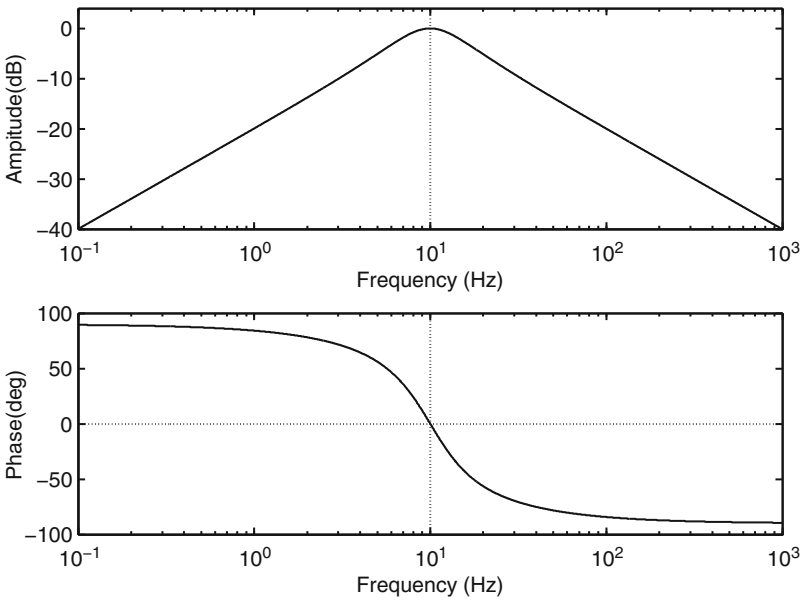

Fig. 6.21 Frequency response of the second band-pass filter when the gain $G = 1$

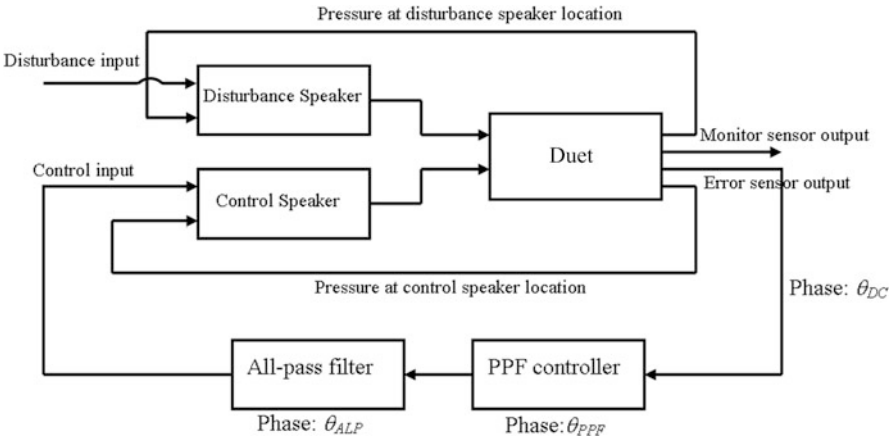

Fig. 6.22 The duct–loudspeaker system with all-pass filter and PPF controller

phase added to the system is a function of several PPF controllers. A second PPF controller placed incorrectly can easily make the first PPF useless. In this study, the band-pass filters are selected as PPF controllers.

As mentioned above, the phase shift due to loudspeaker dynamics should be compensated when the PPF controller is designed. The phase shift of the band-pass filter at ω_c is 0° or 180°. To achieve 180° phase shift of the control path at ω_c, an all-pass filter can be used to adjust the phase of the PPF controller. The closed-loop system is shown in Fig. 6.22. It can be found that there are three phase shifts in the control path, i.e., θ_{DC} is the phase shift from control input to error sensor output, θ_{PPF} is the phase shift of PPF controller, and θ_{ALP} is the phase shift of the all-pass filter.

The transfer function of the all-pass filter, which has the same pole and zero, can be written as

$$H_{AL}(s) = \frac{s - p}{s + p} \tag{6.24}$$

The amplitude response of an all-pass filter is 1 at each frequency, while the phase response (which determines the delay versus frequency) can be arbitrary. Figure 6.23 shows the frequency response of an all-pass filter.

From Fig. 6.22, it is easy to find that the phase of the control path can be written as

$$\theta_c = \theta_{DC} + \theta_{ALP} + \theta_{PPF} \tag{6.25}$$

Assume the frequency of targeted mode is ω_c. If the PPF controller is a low-pass filter,

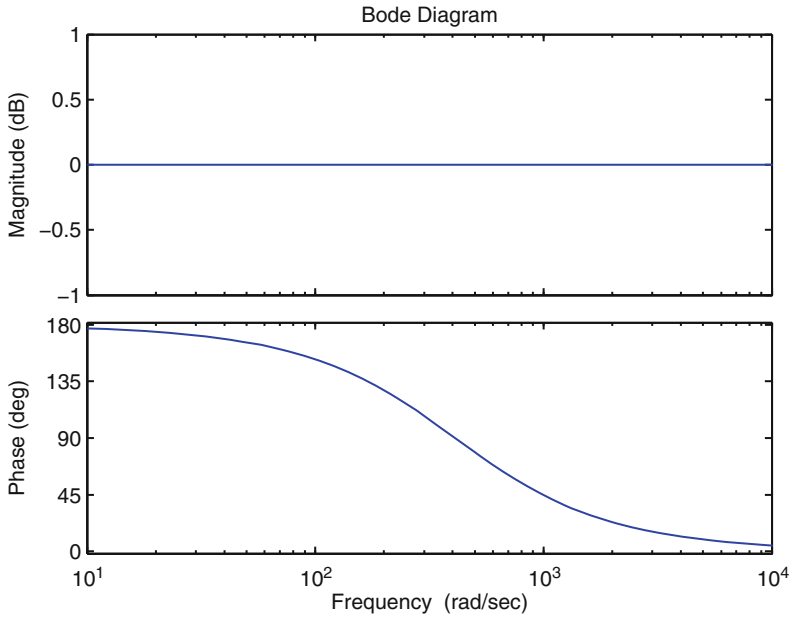

Fig. 6.23 The frequency response of an all-pass filter ($p = 410$ in Eq. (6.24))

$\theta_{\mathrm{PPF}}(\omega_c) = -90°$. If the control source is ideal volume velocity with collocated microphone,
$\theta_{\mathrm{DC}}(\omega_c) = -90°$. This means that $\theta_c(\omega_c) = -180°$ without an all-pass filter.

However, if the loudspeaker dynamics are included, the all-pass filter should be used to guarantee $\theta_c(\omega_0) = -180°$. So the phase of the all-pass filter at ω_c is

$$\theta_{\mathrm{ALP}}(\omega_c) = 180 - \theta_c = 180 - \theta_{\mathrm{DC}} - \theta_{\mathrm{PPF}} \tag{6.26}$$

Notice that the phase shift of the all-pass filter is between $-180°$ and $180°$. If $\theta_{\mathrm{ALP}}(\omega_c) < 0°$, the parameter p in Eq. (6.24) is a negative number. It can be termed as an inversing all-pass filter.

And the parameter p in Eq. (6.24) can be written as

$$p = j\omega_c \frac{1 - \exp\left(j\,\theta_{\mathrm{ALP}}(\omega_c)\right)}{1 + \exp\left(j\,\theta_{\mathrm{ALP}}(\omega_c)\right)} = \frac{\omega_c \sin\left(\theta_{\mathrm{ALP}}(\omega_c)\right)}{1 + \cos\left(\theta_{\mathrm{ALP}}(\omega_c)\right)} \tag{6.27}$$

The size of the rectangular duct (rigid wall) is listed in Table 6.1. One loudspeaker at $x = 0$ is used as primary source, and another loudspeaker at $x = 3.88$ m is

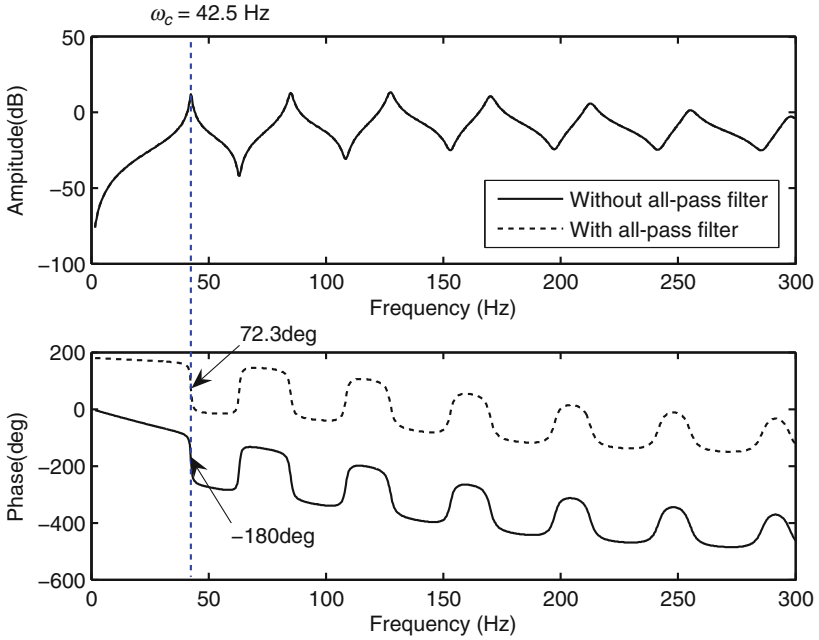

Fig. 6.24 The response of control path

used as a control source. The monitor microphone is located at $x = 4$ m for all cases. First of all, assume the error microphone is at $x = 3.88$ m. A second band-pass filter is used as the PPF controller which is designed to control the first duct mode (natural frequency $\omega_0 = 42.5$ Hz). Figure 6.24 shows the control-path response with and without an all-pass filter. Clearly, without the all-pass filer, the control path cannot guarantee a ± 180 phase shift. Figures 6.25 and 6.26 show the stability analysis of the control path using both root locus analysis and gain and phase margin analysis. It can be found that the instability will appear at 85.8 Hz (the second resonance frequency) with a gain of 2.2 for controller with all-pass filter. So the gain value $G = 1$ is chosen. Figure 6.27 shows the Nyquist diagram for control-path response with and without the all-pass filter. It can be found that the controller without the all-pass filter is unstable when the control gain $G = 1$. After adding the all-pass filter, the gain margin is increased and the system becomes stable. Figure 6.28 shows the pressure measured by the monitor microphone using a PPF controller with an all-pass filter. From Fig. 6.28, it can be found that 14 dB reduction can be obtained. However, there are 6 and 4 dB increases at the second and third resonance modes.

For simplicity, in the following sections, the PPF controller with optimal all-pass filter will be abbreviated as phase-compensated PPF controller. If we consider controlling the third acoustic mode at 127.5 Hz (the third mode), Fig. 6.29 shows the root locus analysis of the control path. It can be found that the instability will

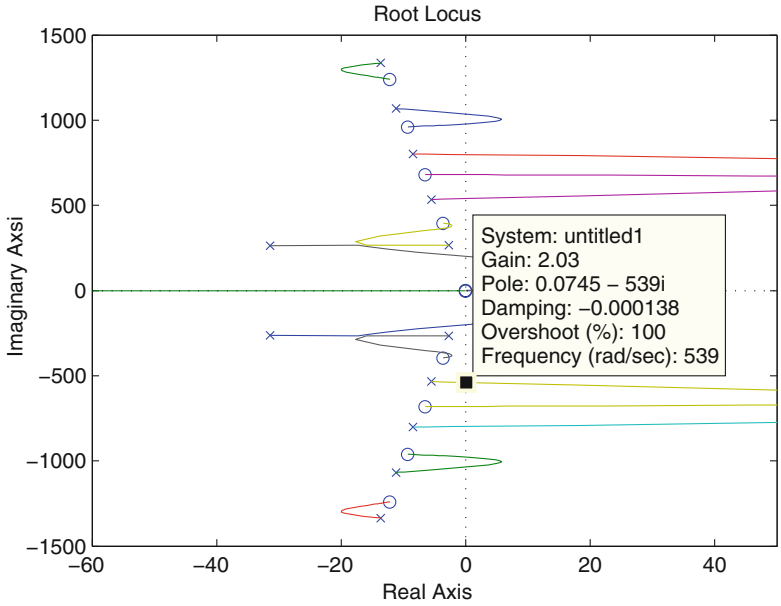

Fig. 6.25 The root locus analysis of control path with all-pass filter

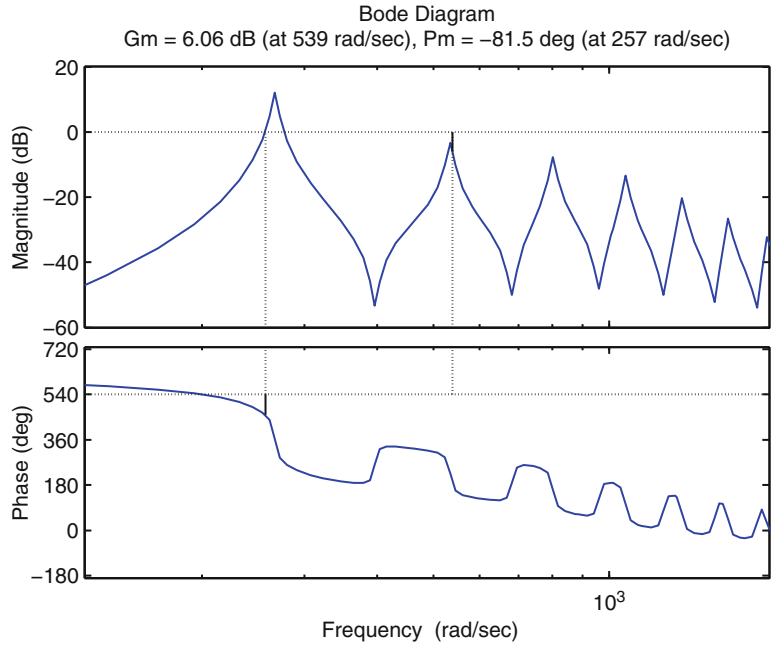

Fig. 6.26 The gain and phase margin of control path with all-pass filter

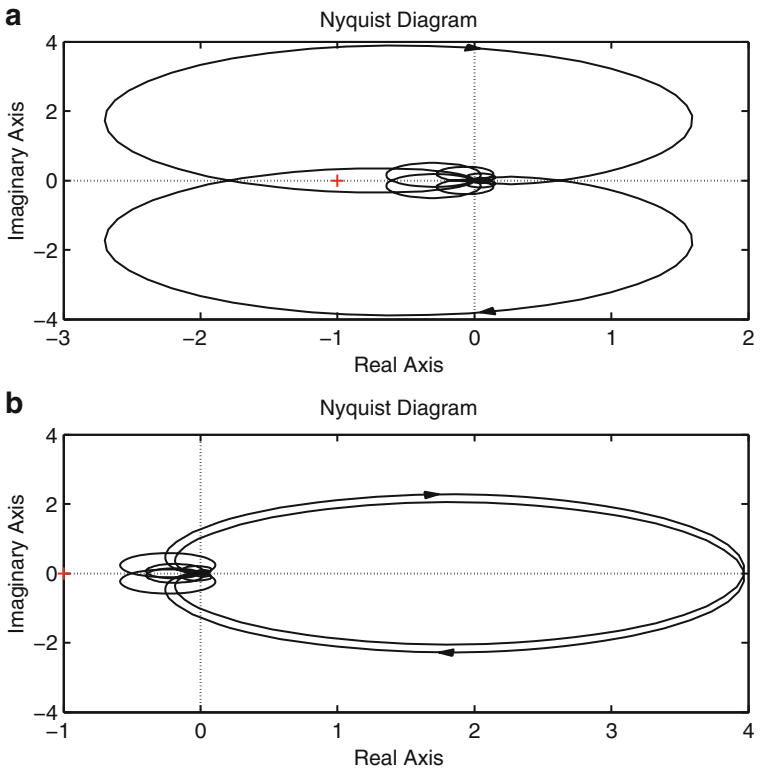

Fig. 6.27 The Nyquist diagram of control path when the control gain = 1. (**a**) Without all-pass filter; (**b**) with all-pass filter

appear at 83.7 Hz with gain 3.7. So the gain $G = 0.6$ is chosen. Figure 6.30 shows the pressure measured by the monitor microphone using a phase-compensated PPF controller. Notice that 11 dB reduction is achieved at the third mode. However, there are 2.8 and 1.6 dB increases at the second and fourth resonance modes.

The ideal phase-compensated PPF controller only controls the target mode without influencing other modes. To improve the performance of the phase-compensated PPF controller, we can use higher-order filter (such as a fourth-order Butterworth filter) instead of the second-order filter to control the first mode of the duct. Figure 6.31 shows the response of the fourth-order Butterworth band-pass filter, which has 50 dB/dec of attenuation on both sides of the center frequency. Figure 6.32 shows the root locus analysis of the phase-compensated PPF controller. The instability occurs at 38 Hz with gain 3.6. Comparing with Fig. 6.25, it can be found that the maximum allowable gain increases from 2.2 to 3.6. So we choose the gain $G = 1$ for the control path. Figure 6.33 shows the Nyquist diagram. Notice that the stability can be guaranteed with gain $G = 1$. Figure 6.34 shows the pressure

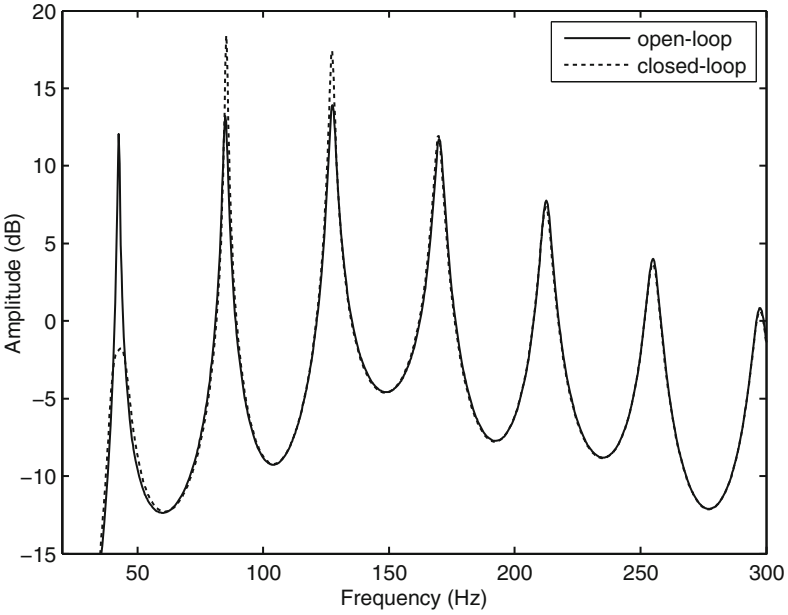

Fig. 6.28 The pressure at monitor sensor

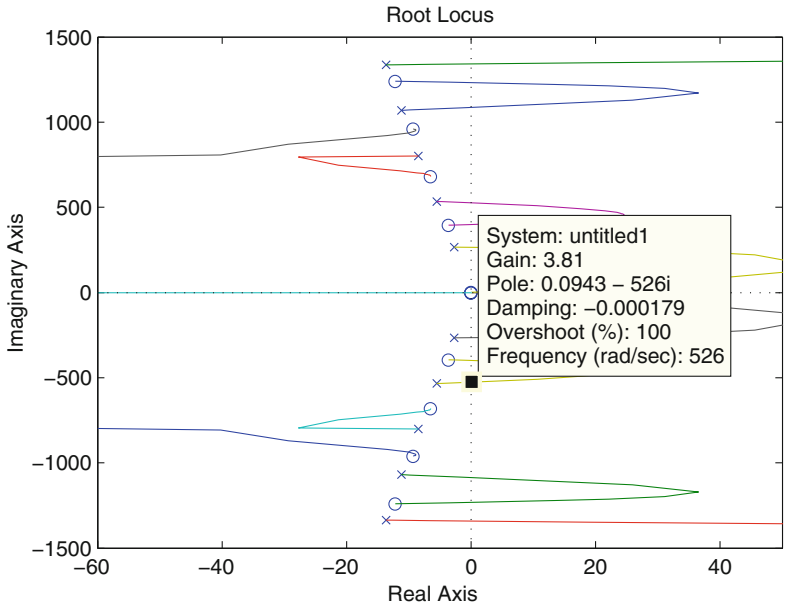

Fig. 6.29 The root locus analysis of the control path

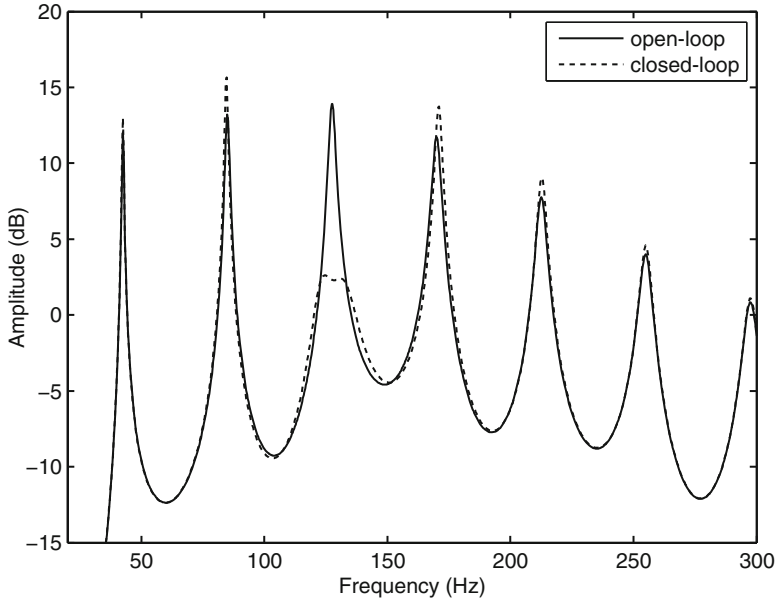

Fig. 6.30 The pressure at monitor sensor

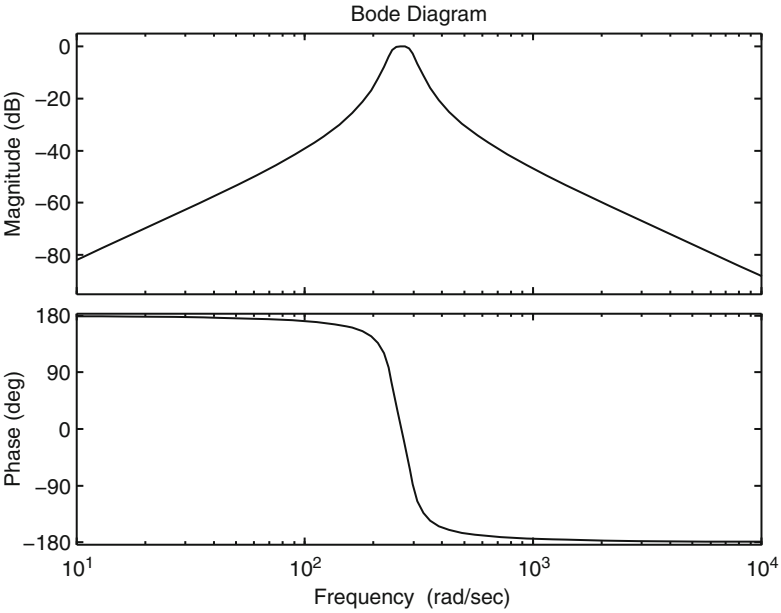

Fig. 6.31 The frequency response of a fourth band-pass filter

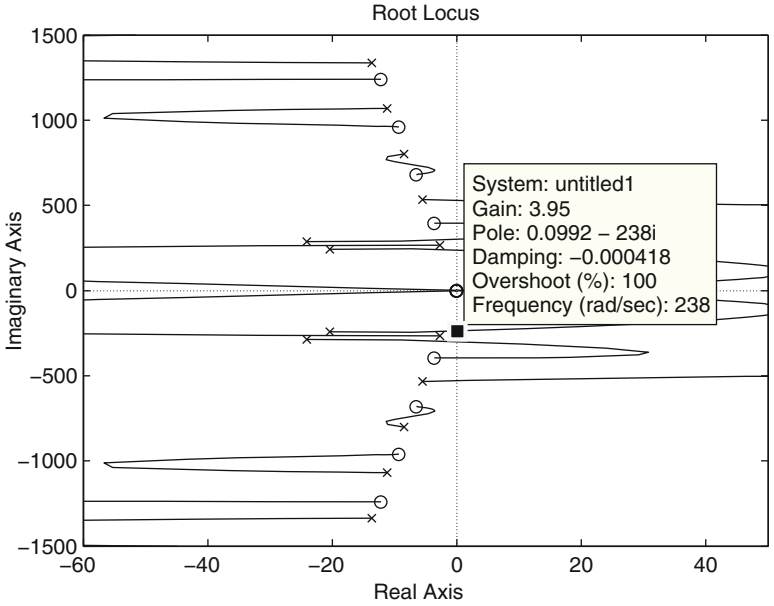

Fig. 6.32 The root locus analysis of the phase-compensated PPF controller using the fourth-order Butterworth band-pass filter

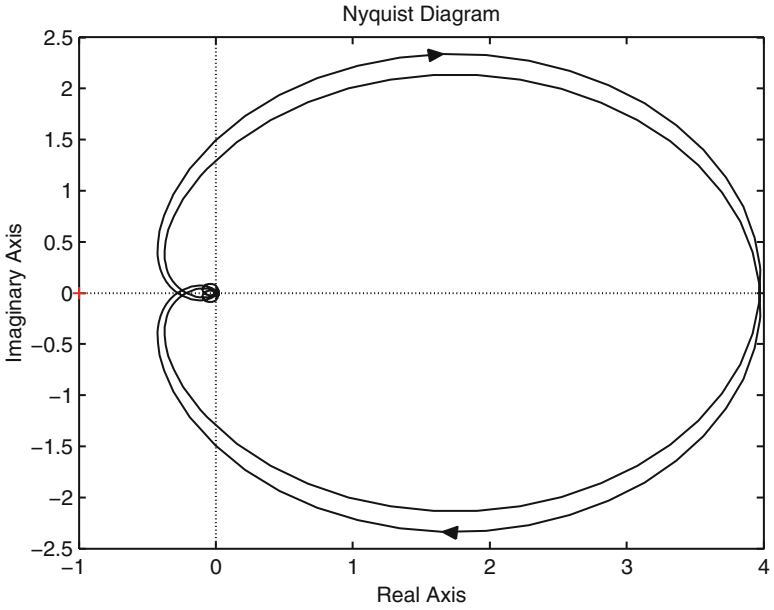

Fig. 6.33 The Nyquist diagram of phase-compensated PPF controller

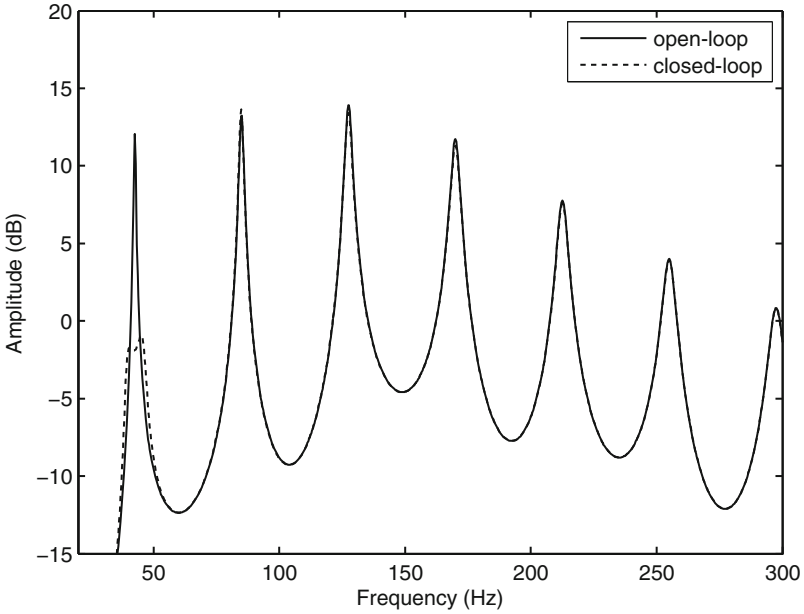

Fig. 6.34 The open-loop and closed-loop responses at monitor sensor by using fourth band-pass filter

of monitor sensor with phase-compensated PPF controller by using a fourth-order Butterworth filter. It can be found that a 14 dB reduction can be obtained and without influence at other modes.

The spatial frequency responses of the uncontrolled and controlled duct are shown in Fig. 6.35. It is observed that the resonance response of the first mode has been reduced over the entire duct due to the phase-compensated PPF controller action. The resonance response of the first mode has been reduced by approximately 12 dB over the entire duct.

6.4 Non-collocated Loudspeaker/Microphone Pair

One of advantages of this type of phase-compensated PPF controller is that the error microphone can be non-collocated, because the phase can be shifted by an all-pass filter. Assume that a second-order filter with bandwidth 10 Hz is used to control the first acoustic mode when the error microphone is located at $xs = 0.6$ m and control loudspeaker is located at $xc = 3.88$ m. Figures 6.36 and 6.37 show the root locus analysis and Nyquist diagram with gain $G = 1$. Comparing with Fig. 6.25,

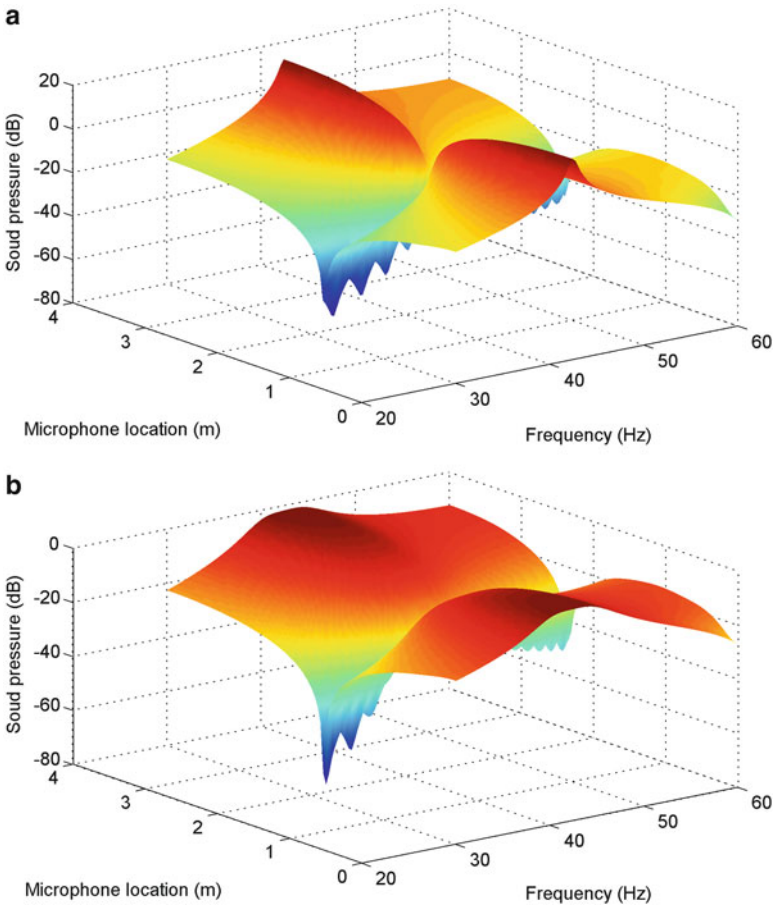

Fig. 6.35 The spatial frequency responses. (**a**) Before control; (**b**) after control

the maximum allowable gain is increased from 2.2 to 15.1. Figure 6.38 shows the control path with and without an all-pass filter. Similar to the collocated case, the phase shift at the targeted mode is a multiple of 180°. Figure 6.39 shows the open-loop and closed-loop responses of the monitor sensor. It can be found that 14 dB-reduction is achieved at the first mode, and there is 2 dB-reduction at the second mode.

Figure 6.40 shows the closed-loop response and Nyquist diagram with different control gain (second-order PPF controller, bandwidth = 10 Hz). It can be found that larger gain can obtain better reduction; however, if the gain is too large, the system will become unstable. Selecting a reasonable gain is an important issue when designing a PPF controller.

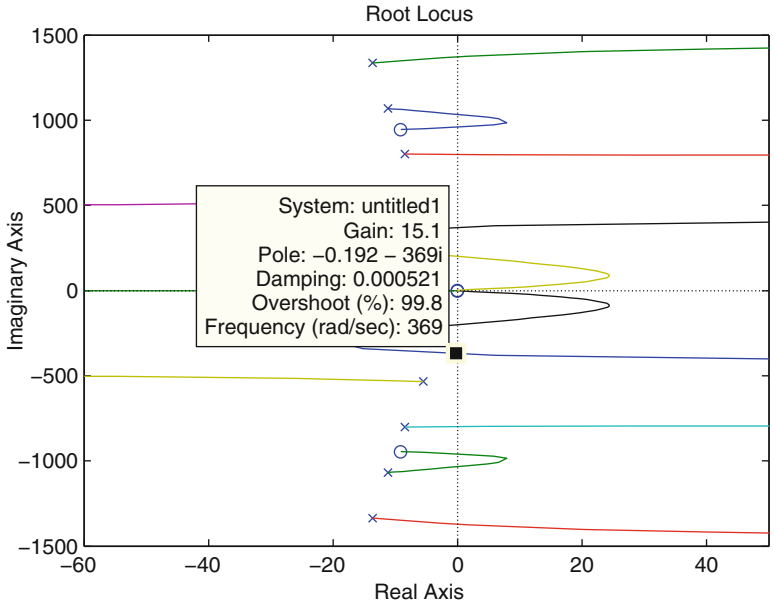

Fig. 6.36 The root locus analysis of the phase-compensated PPF controller

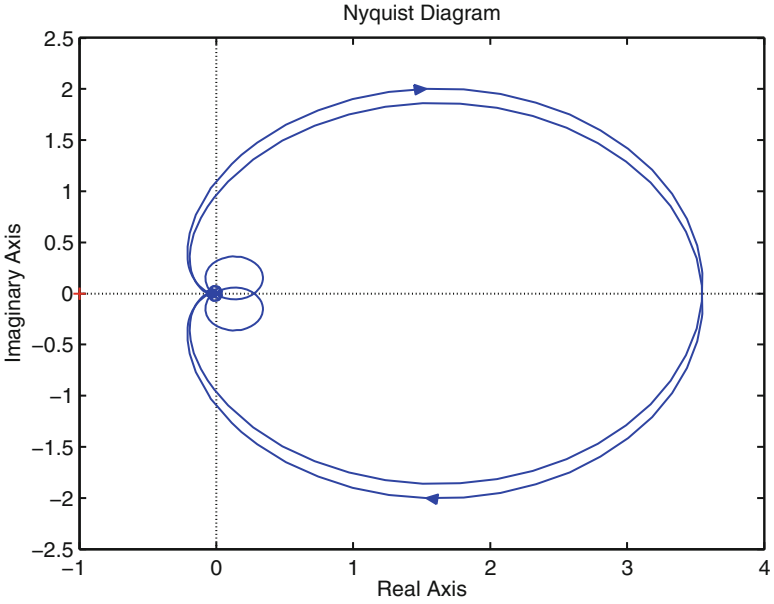

Fig. 6.37 The Nyquist diagram of the phase-compensated PPF controller

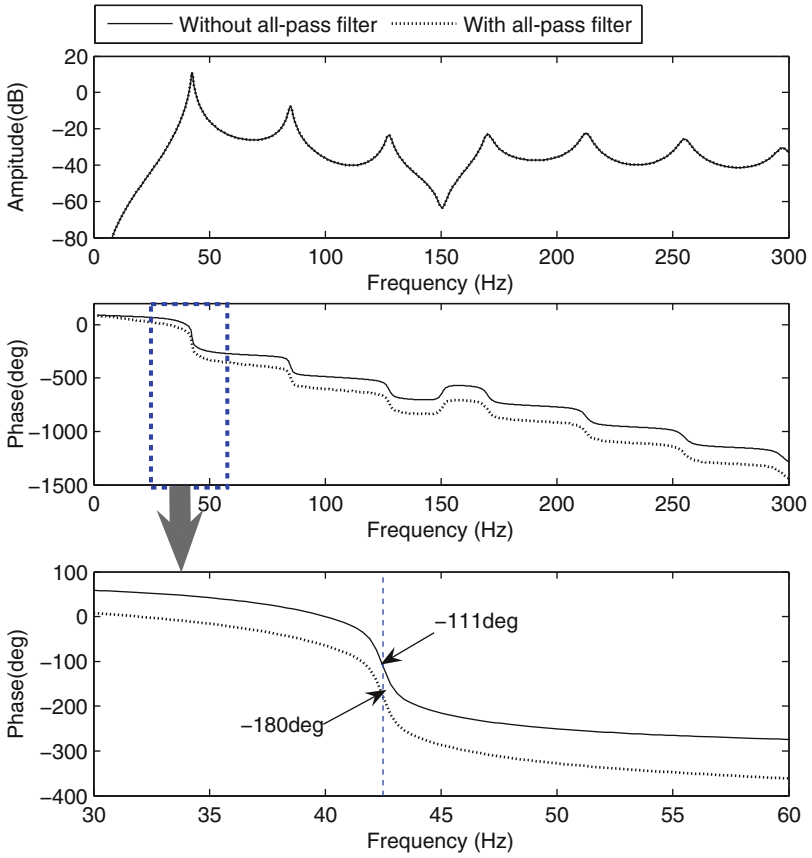

Fig. 6.38 The response of the control path with and without all-pass filter

6.5 Multimode Control

In this section, by using a single control loudspeaker and error microphone pair, we discuss the multimode control using phase-compensated PPF controller networks. Each phase-compensated PPF controller is independently tuned to the different acoustic mode. The PPF phase-compensated controllers are connected in parallel, and the voltage outputs are summarized to the control loudspeaker, as illustrated in Fig. 6.41.

In order to effectively realize the multimode control, the modal spacing should be sufficiently large. Otherwise, the PPF controllers cannot be designed independently due to the overlapping phases of PPF controllers. In this study, the modal spacing is 42.5 Hz and it is sufficiently large to independently design the PPF controller networks. The first three acoustic modes, $\omega_1 = 42.5$ Hz, $\omega_2 = 85.0$ Hz, and $\omega_3 = 127.5$ Hz, are the design modes to be controlled. Assume that the error microphone is located at $\mathrm{xs} = 0.5$ m and the control loudspeaker is located at

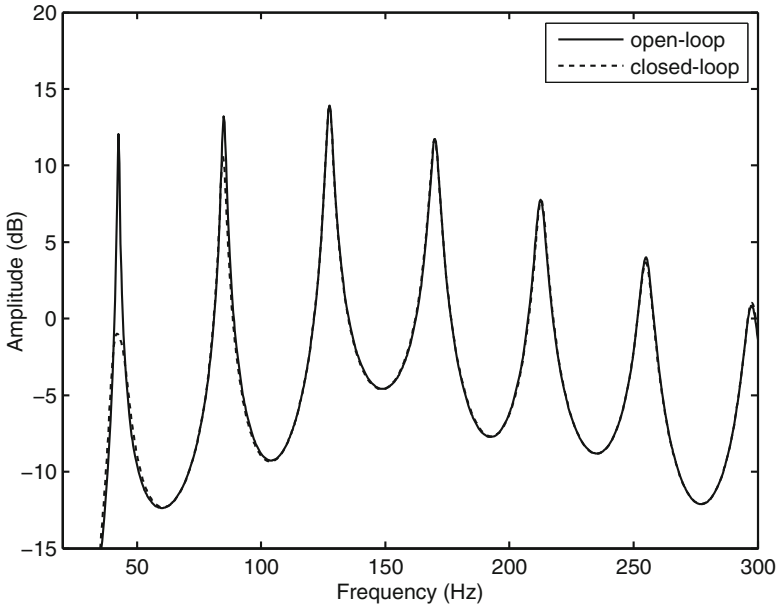

Fig. 6.39 The open-loop and closed-loop responses of the monitor sensor

xc = 3.88 m. Here we choose three second-order band-pass filters as controllers, where the gain of each PPF controller is 1, and the bandwidths are 10 Hz, 15 Hz, and 20 Hz for mode-1, mode-2, and mode-3 controllers, respectively. Figure 6.42 shows the frequency response of the control path. It can be found that slight phase shift errors occur due to the overlapping phases of phase-compensated PPF controllers. The phase shift at each resonance frequency is 176.5°, 177.5°, and 170.3°, respectively. Since the errors are less than 10° from the required 180°, the phase-compensated PPF controllers can be seen independent of each other. Figure 6.43 shows the Nyquist diagram for the control path. Notice that the control system is stable. Figure 6.44 shows the closed-loop response. A 13 dB reduction is seen in the first and second modes and 9.5 dB reduction at the third mode.

6.6 Sharing Data Between Simulink and the GUI

Simulink is a software package for modelling, simulating, and analyzing dynamic systems. It supports linear and nonlinear systems, modelled in continuous time, sampled time, or a hybrid of the two. In this section, we discuss how to share the data between Simulink and a GUI program.

The Simulink program ***ppf_nduct_c.mdl***, as illustrated in Fig. 6.45, is used to analyze the loudspeaker–duct model using a single phase-compensated PPF

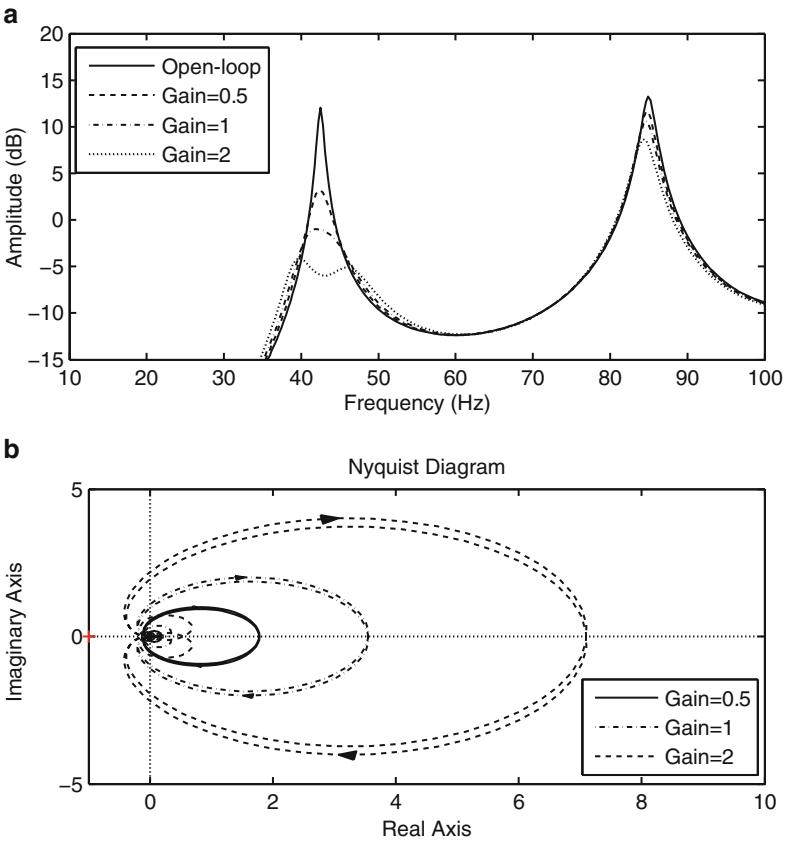

Fig. 6.40 (**a**) The closed-loop response and (**b**) Nyquist diagram with different control gain for the phase-compensated PPF controller

controller. It should be noticed that this Simulink program requires to read data from workspace. It means that before we run this Simulink program, we should run ***Ch_6_24_28.m***, ***Ch_6_31_34.m*** or ***Ch_6_36_39.m***, because these MATLAB file will save necessary data into workspace for Simulink program. One case of the time response of loudspeaker–duct model before and after control is shown in Fig. 6.46.

Finally, a GUI program (with files ***ppf_00.m*** and ***ppf_00.fig***) is given to illustrate the design of a PPF controller. The interface of the GUI program is shown in Fig. 6.47. In this program, the locations of the error microphone, monitor microphone, and control speaker can be adjusted, and we can select the type of band-pass filter (such as Butterworth, Chebyshev type I, Chebyshev type II, and Elliptic filter) as PPF controller. On the right side of the interface, the parameters of PPF controller (such as target mode, order of controller, bandwidth, and gain of controller) can be adjusted. If you push the "Compute" push button, the program will automatically check the stability of the control system. The control-path response,

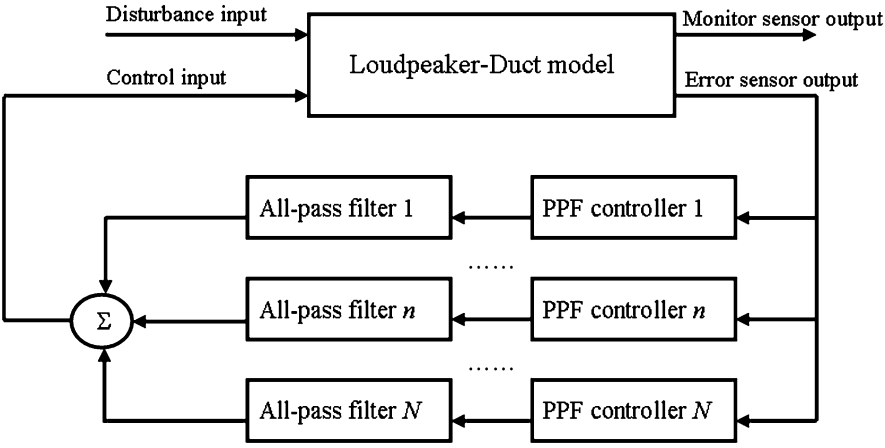

Fig. 6.41 The duct–loudspeaker system with phase-compensated PPF controller networks

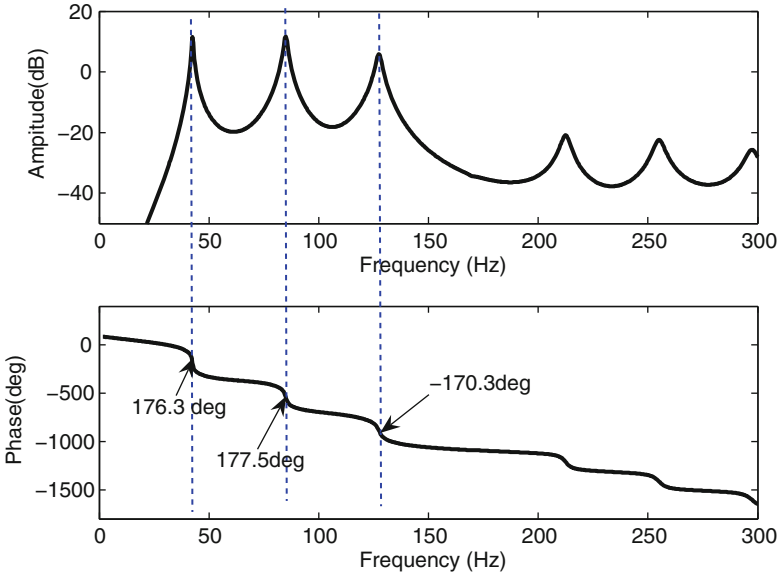

Fig. 6.42 The frequency response of the control path

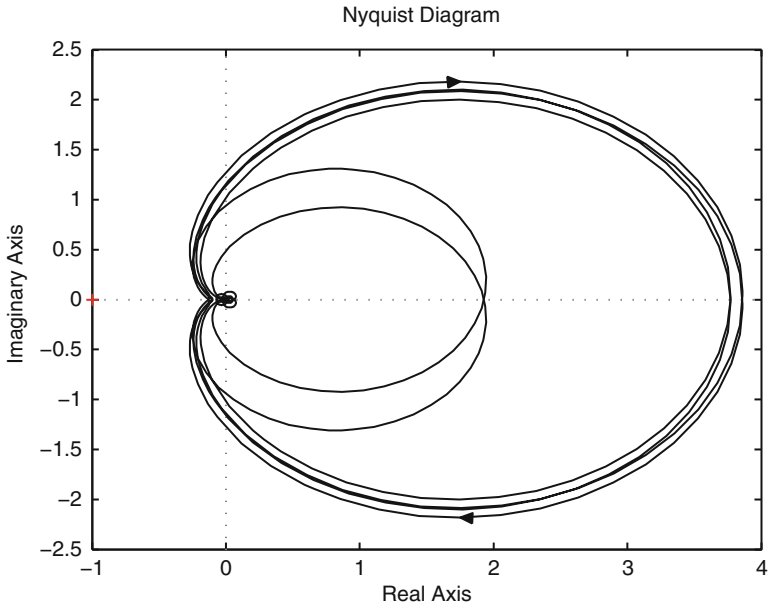

Fig. 6.43 The Nyquist diagram for the control path

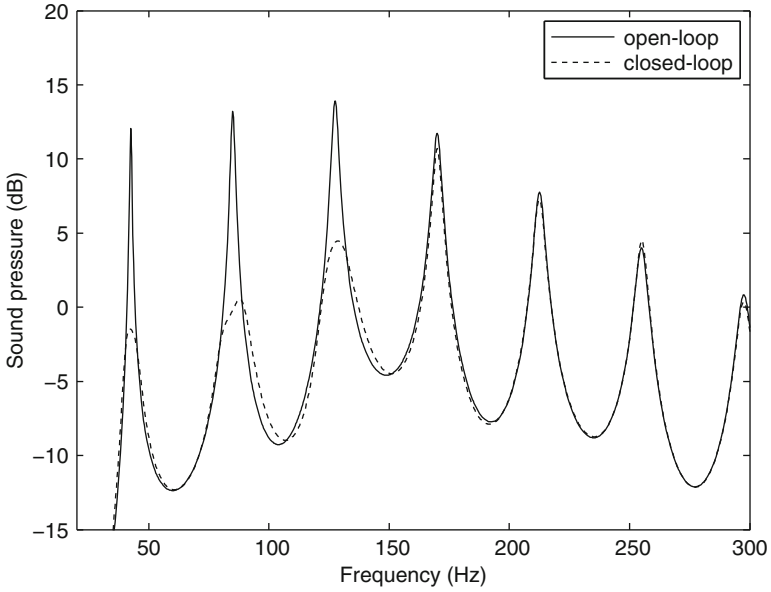

Fig. 6.44 The closed-loop response using phase-compensated PPF controller networks

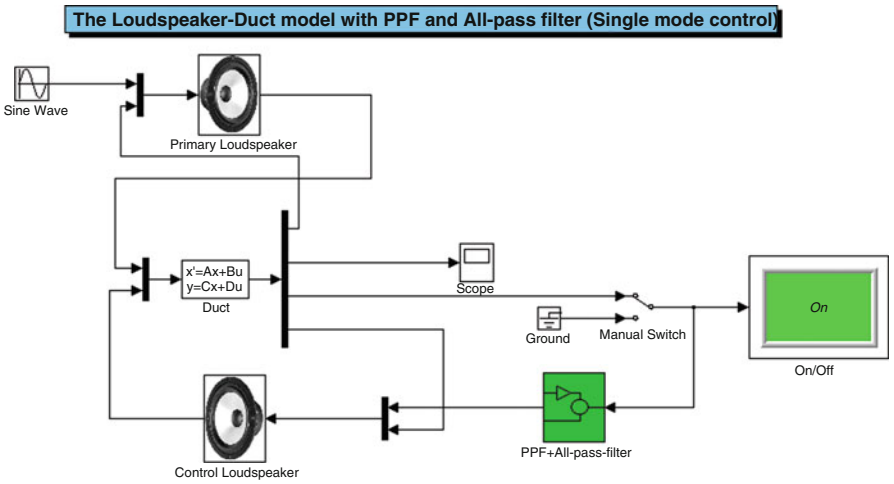

Fig. 6.45 The Simulink model for single mode control case

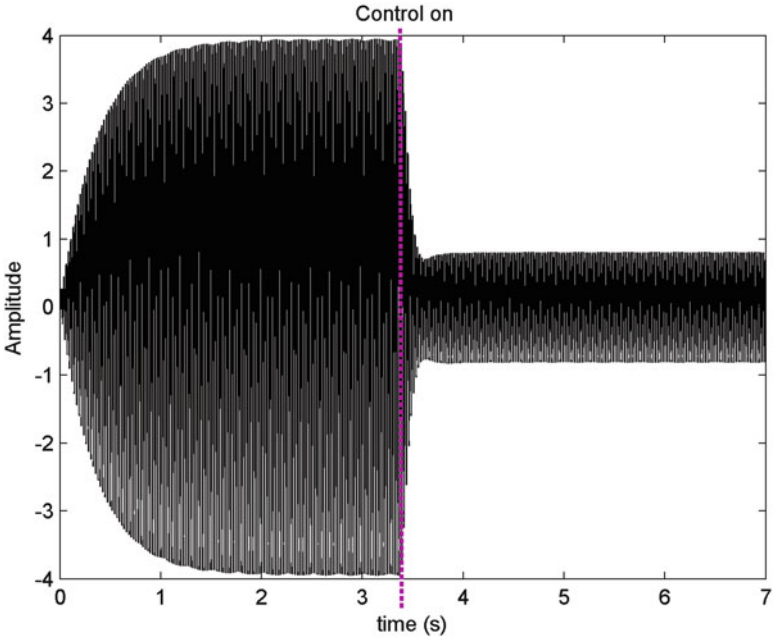

Fig. 6.46 The time response of loudspeaker–duct model

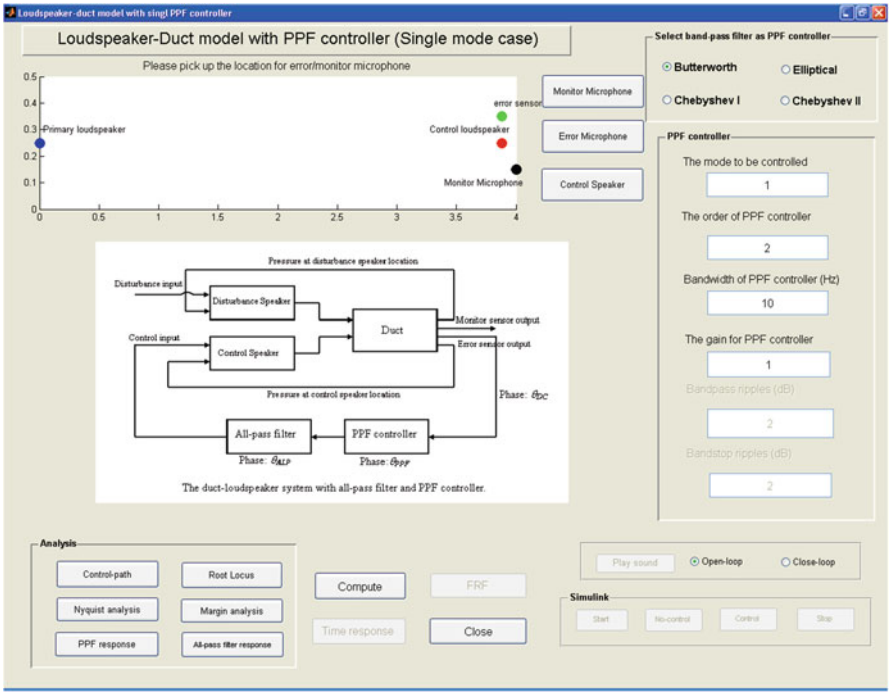

Fig. 6.47 The interface of the GUI program for the single mode control case

Nyquist diagram, root locus analysis, and margin diagram are given. Figure 6.48 presents the results when you push the different push buttons. The frequency response of the band-pass filter will automatically show on the interface when you change the parameters of the filter. And the closed-loop response is also immediately presented when the monitor microphone location is changed.

At the bottom-right of the GUI interface, the push button "Play sound" presented as Fig. 6.49 is used to play the sound at target resonance frequency. The sound is played from the Simulink program by using the parameters in current GUI. It should be noted that the sound may be very low if you select the first mode (natural frequency is 42.5 Hz) for normal computer speakers. The sound can be heard clearly for other modes.

The "Simulink" push button group shown in Fig. 6.50 is used to run the Simulink model "ppf_nduct_2.mdl" in the GUI program. The control on/off can be selected with the online sound play.

Now we discuss how to share the data between Simulink and the GUI program. Table 6.4 lists several Simulink functions used in the GUI program.

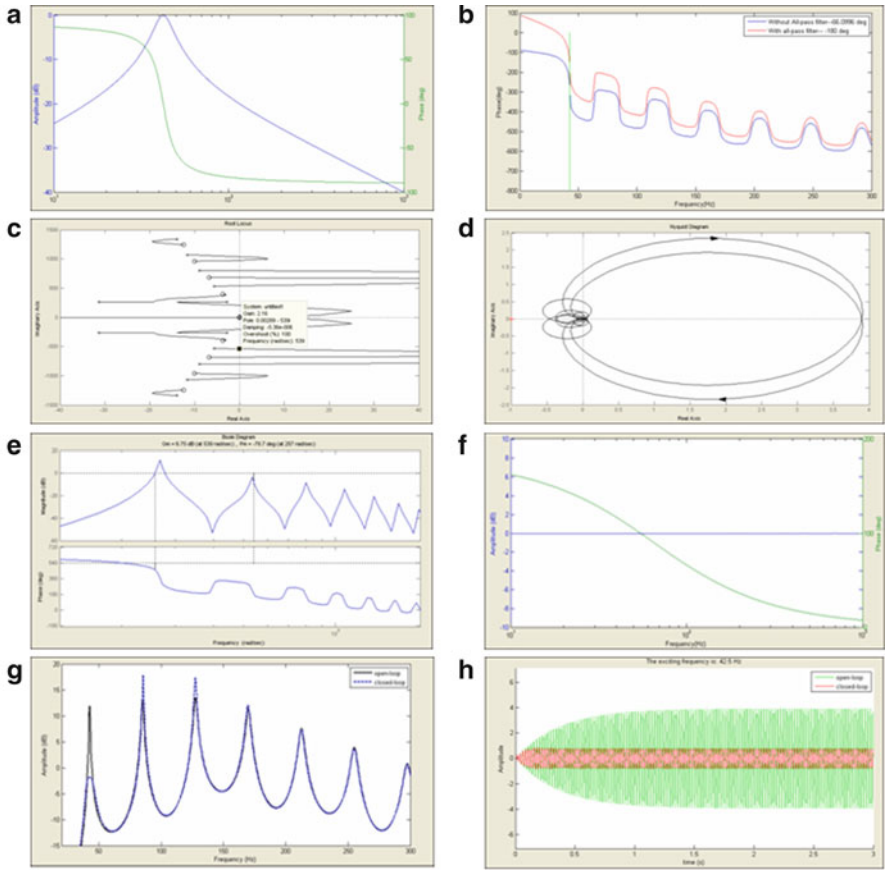

Fig. 6.48 The results for different push buttons shown in Fig. 6.46. (**a**) PPF response; (**b**) control path; (**c**) root locus; (**d**) Nyquist analysis; (**e**) margin analysis; (**f**) all-pass filter response; (**g**) FRF; (**h**) time response

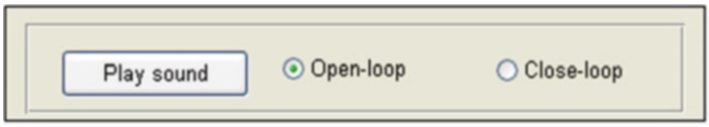

Fig. 6.49 The push button "Play sound"

Fig. 6.50 The Simulink push button group

Table 6.4 Several Simulink functions used in the GUI program

Functions	Description
Sim	To execute a Simulink model
open_system	To open a Simulink system window or a block dialog box
set_param	To set Simulink system and block parameters
save_system	To save a Simulink system
close_system	To close a Simulink system window or a block dialog box

This example is designed to work with the loudspeaker–duct Simulink model. Since the GUI sets parameters and runs the simulation, the Simulink model will be open when the "Start" button is pushed. The purpose of the "Start" push button is to:

- Determine if the model is open (**find_system**)
- Open the block diagram for the model and the subsystem where the parameters are being set, if not open already (**open_system**)
- Update the parameter of the controller to match the current settings in the GUI (**set_param**)
- Bring the GUI forward so it is displayed on top of the Simulink diagrams (**figure**)
- Update the Simulink program actions to match the current settings in the GUI (stop, control on/off)

Below we present the function "**Start_Callback**" which is used to open the Simulink model and update the parameters according to current setting in GUI.

```
% --- Executes on button press in Start.
function Start_Callback(hObject, eventdata, handles)
% hObject    handle to Start (see GCBO)
% eventdata  reserved - to be defined in a future
  version of MATLAB
% handles    structure with handles and user data
  (see GUIDATA)
% Hint: get(hObject,'Value') returns toggle state of
  Start global HHH
if  isempty(find_system('Name','ppf_nduct_2')),
    open_system('ppf_nduct_2');
end
HHH=0;assignin('base','HHH',HHH);
set_param('ppf_nduct_2','simulationcommand','update');
open_system('ppf_nduct_2/Scope')
set(handles.togglebutton3,'enable','on');
set(handles.togglebutton4,'enable','on');
set(handles.Stop          ,'enable','on');
```

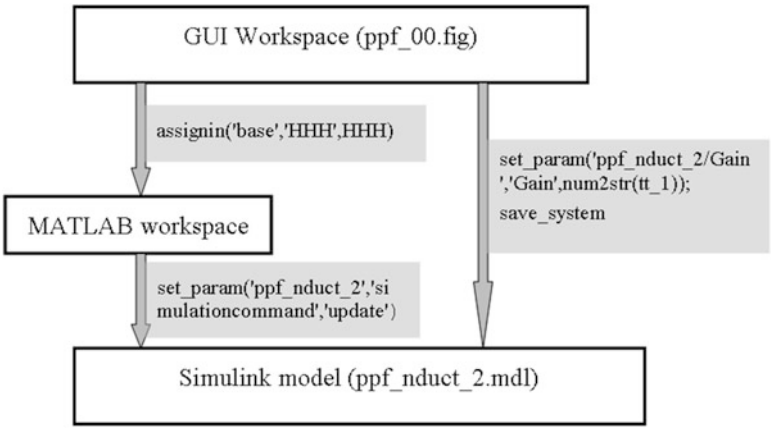

Fig. 6.51 Share the data between GUI and Simulink model

```
tt_1 = str2double(get(handles.edit1,'String'))*0.1;
set_param('ppf_nduct_2/Gain','Gain',num2str(tt_1));
save_system

HHH=0;
if get(handles.Start,'Value')==1
    set(handles.togglebutton3,'Value',1)
set_param('ppf_nduct_2','simulationcommand','start');
end
```

In this function, we use two methods to update the Simulink model, as shown in Fig. 6.51. One method is to use the command "**set_param**" which sets the specified model parameters to the specified values. In our GUI program, almost all parameters of Simulink model will be changed when we move the monitor/error microphone locations. The program will be very slow if using the command "**set_param**" to update the Simulink model. An alternative method is to use the command "**assignin**" to save the variable from the GUI workspace to the MATLAB workspace, then update the model.

Another GUI program (with files ***ppf_01.m*** and ***ppf_01.fig***) is used to compute the multimode control case, as shown in Fig. 6.52. Similar to the single mode control GUI program, the locations of error microphone, monitor microphone, and control speaker can be adjusted. The parameters of PPF controller (such as target mode, order of controller, bandwidth, and gain of controller) can be adjusted. However, this GUI focuses on the multiple mode control. On the right interface, we can input multiple modes to control, as illustrated in Fig. 6.53 (first three modes are targeted).

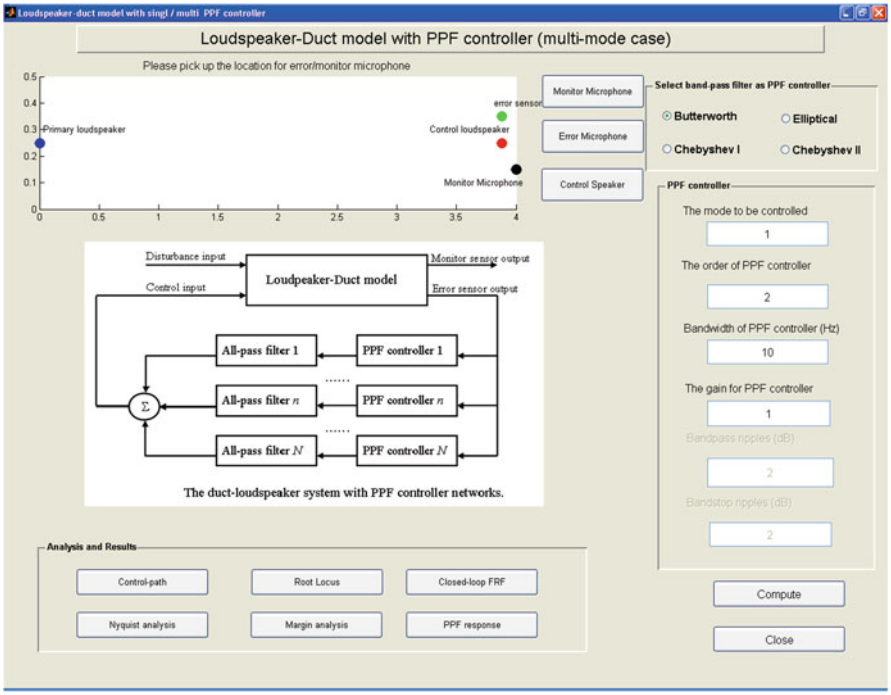

Fig. 6.52 The interface of the GUI program for multimode PPF controllers

Figure 6.54 shows the control-path response and closed-loop response. It can be found that slight phase shift errors at targeted resonance frequencies occur due to the overlapping phases of PPF controllers. However, the closed-loop response shows that the sound pressures at targeted modes are reduced significantly.

6.7 Analog Circuit Design and Experimental Setup

In this section, the experimental setup is verified. Two experimental controllers are developed and applied to a rigid-wall duct with two loudspeakers. Figure 6.55 shows the all-pass filter circuit. This circuit includes three parts, i.e., voltage follower, all-pass filter, and inverse amplifier. In this case, the gain of the inverse amplifier is 1; it is used to shift phase 180°. By using this circuit, the phase can be shifted from 180° (output_1) to −180° (output_2). From Fig. 6.55, it is easy to find that pole/zero p in Eq. (6.24) can be written as

$$p = \frac{1}{C_{\mathrm{a}} R_{\mathrm{b}}} \tag{6.28}$$

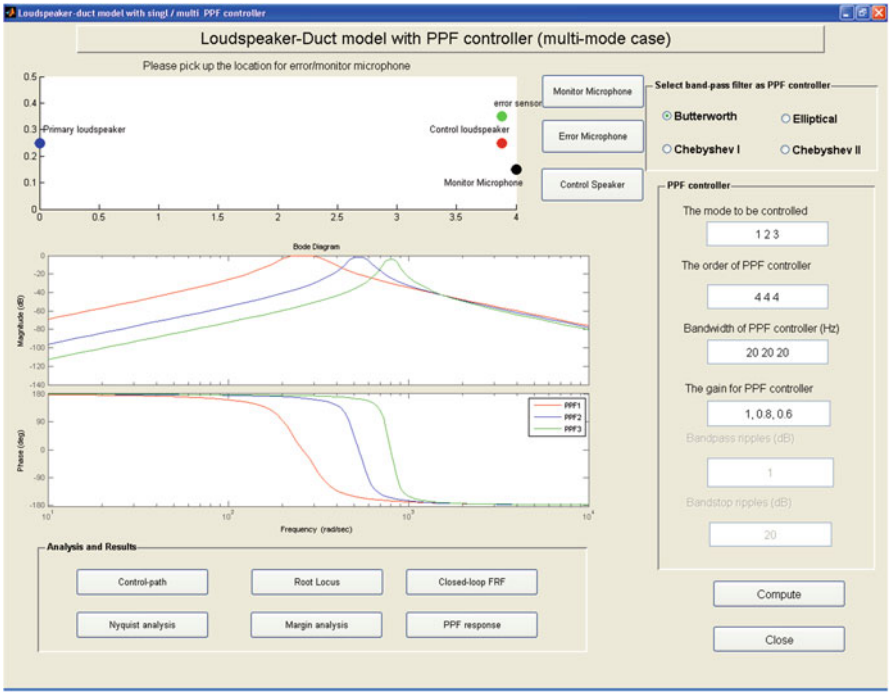

Fig. 6.53 The parameters for multimode PPF controller

In this experiment, the Butterworth analog second-order band-pass filters are used. These filters are made of Burr-Brown (BB) UAF42AP universal filters. Figure 6.56 shows the UAF42AP operational amplifier, which is used as the band-filter. The natural frequency of the band-filter can be determined using the BB Filter42 design program [14]. Figure 6.57 shows the band-pass filter design diagram using UAF42AP.

6.8 Experimental Results

Firstly, the end of the duct is opened. According to the measured frequency response function (FRF), we use PPF controller to control the second mode of this duct. The natural frequency of the second mode is at 182 Hz. Figure 6.58 shows the experimental and simulated band-filter response.

According to our calculation, it is found that the all-pass filter should shift 77° at 182 Hz. Figure 6.59 shows the all-pass filter response. The simulated results agree well with experimental results. Figure 6.60 shows the control-path response with

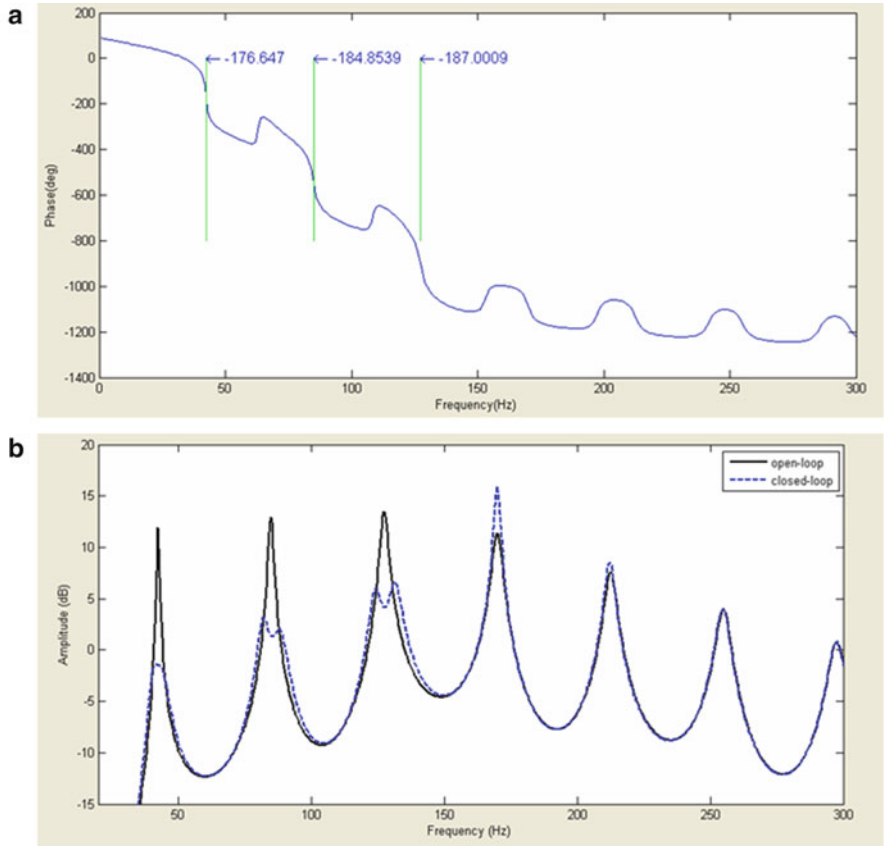

Fig. 6.54 Selected results of GUI program. (**a**) Control-path response; (**b**) closed-loop response

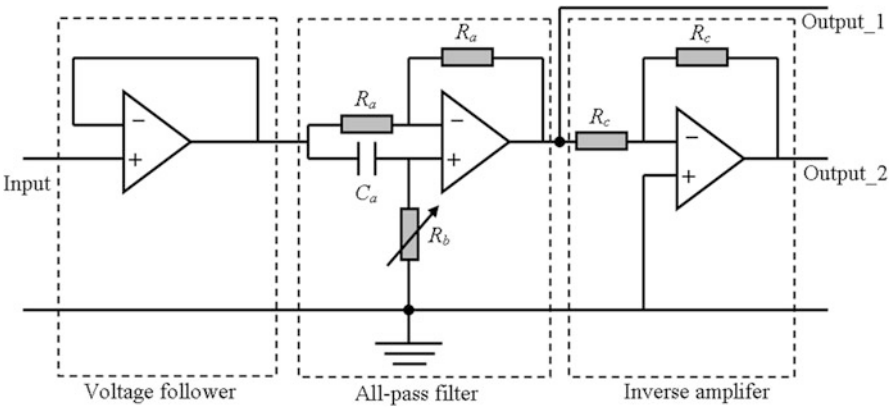

Fig. 6.55 All-pass filter

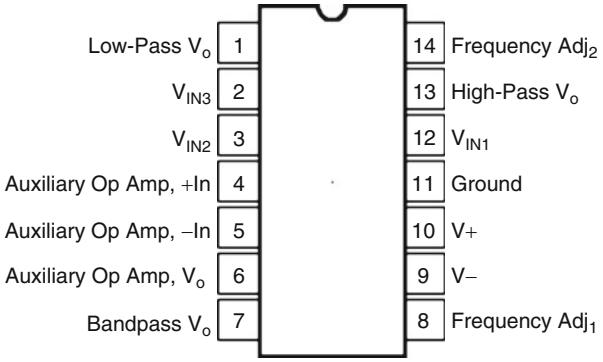

Fig. 6.56 The operational amplifier UAF42AP (From Burr-Brown Co.)

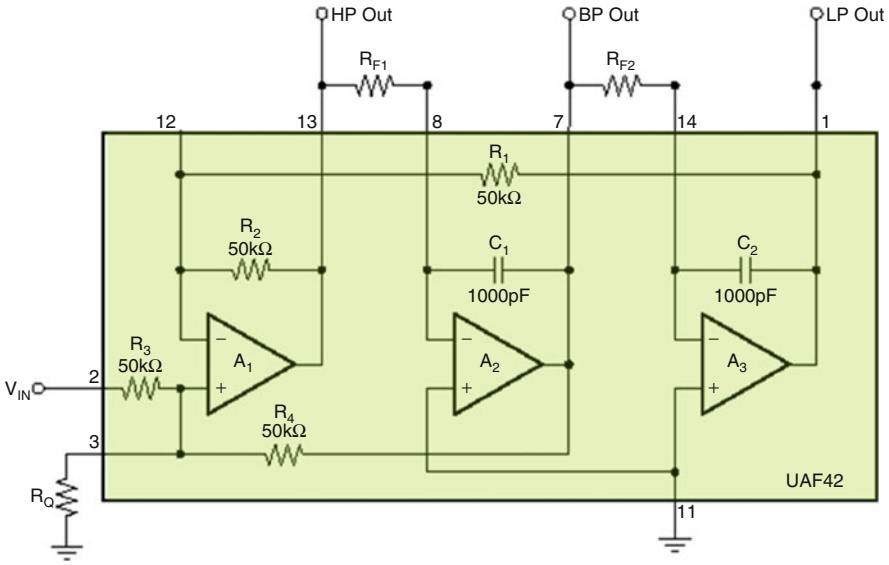

Fig. 6.57 Design the low-pass and band-pass filter

and without an all-pass filter. Clearly, after adding the all-pass filter, the phase of the control path at 182 Hz is −181°. It is almost the same as we expected (180°). Figure 6.61 shows the measured FRF with and without control. Twelve decibels (12 dB) reduction can be observed around the second mode. It should be noted that the error microphone and control loudspeaker is not collocated. This is the main advantage of this type of PPF controller, because the microphone can be located at any location.

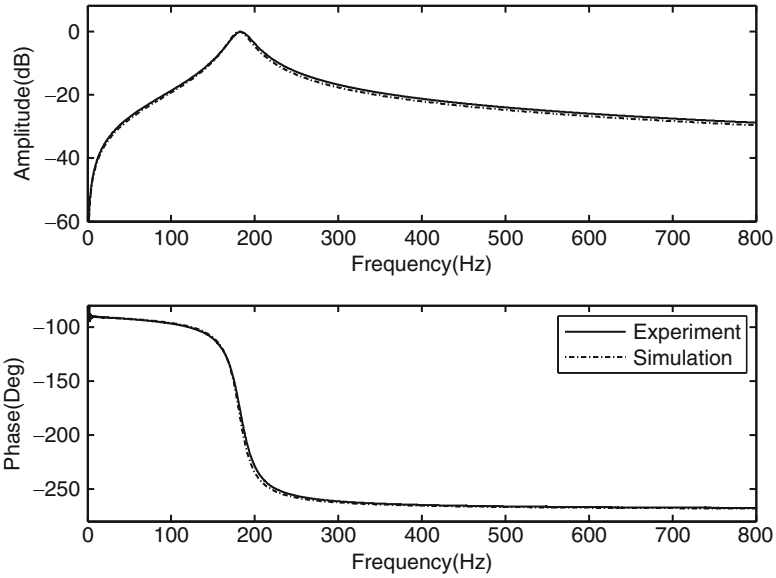

Fig. 6.58 Response of PPF controller

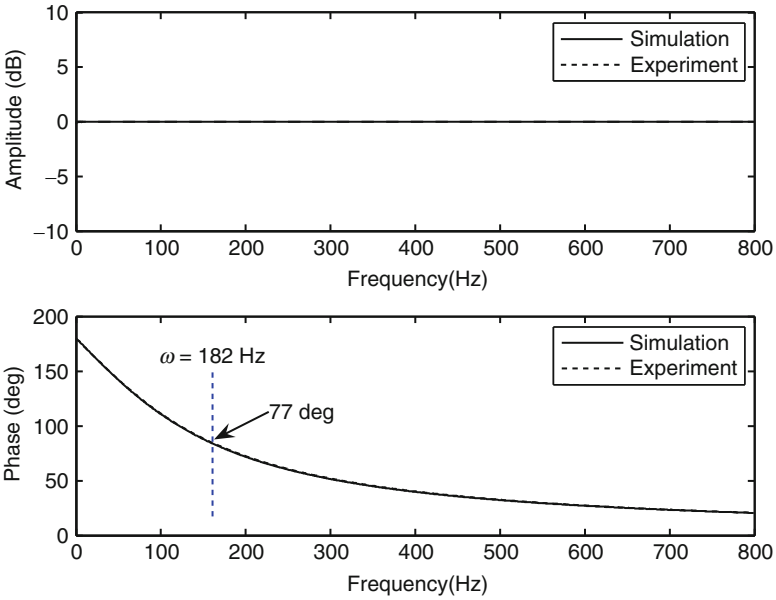

Fig. 6.59 The response of all-pass filter

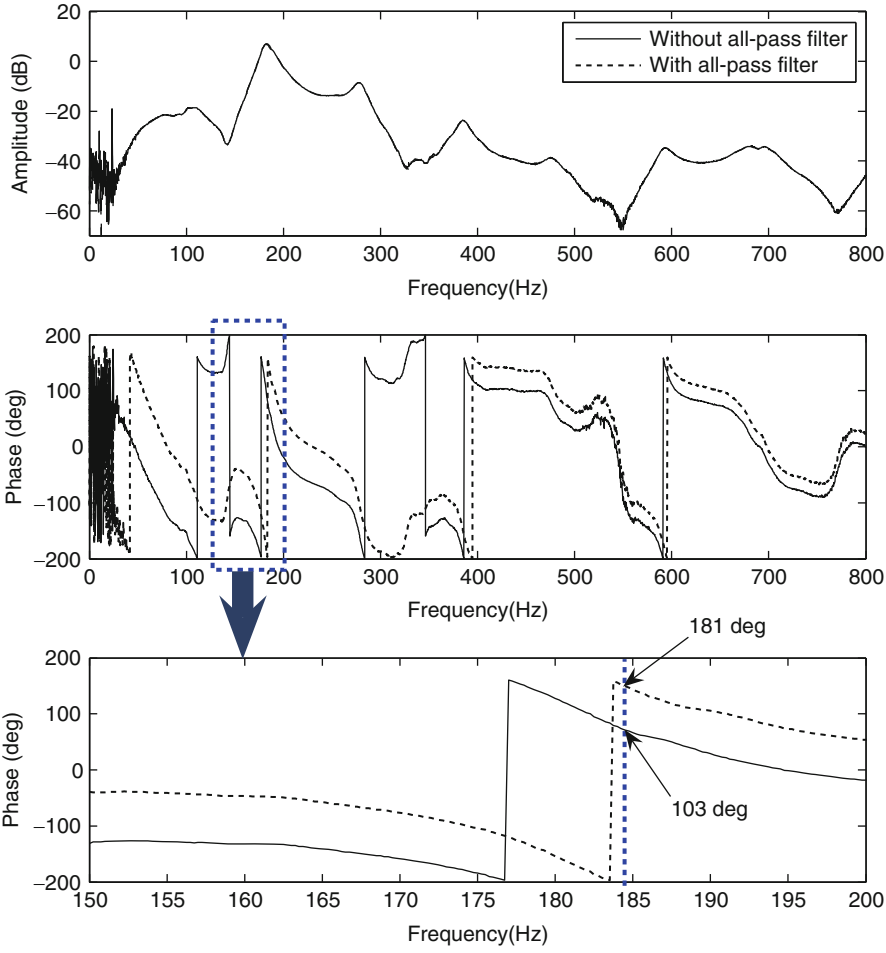

Fig. 6.60 Control path with and without all-pass filter

To further investigate the control performance of this PPF controller, the end of the duct is covered with a rigid plate. Two control cases are presented: one is by using one loudspeaker and one microphone (Case A); another case is by using two control loudspeakers and two microphones (Case B). The control loudspeakers are excited with the same control signal from one PPF controller, and the microphones signals are added together then inputted to the PPF controller. Figure 6.62 shows the control performance for a rigid duct. By using two loudspeakers, the PPF controller has a large influence on the untargeted modes (modes 1, 3, and 4).

The experimental results show that the PPF controller with an all-pass filter can reduce the sound pressure of the duct significantly for the non-collocated microphone/loudspeaker case.

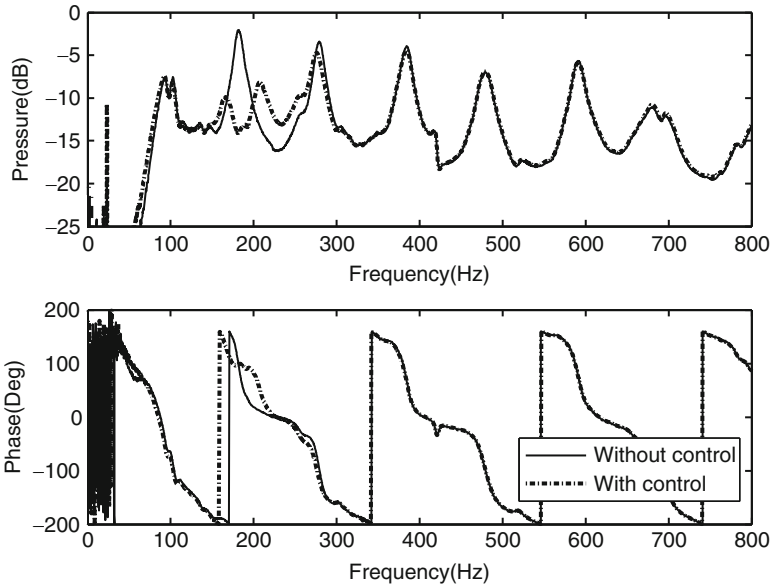

Fig. 6.61 The control performance of the PPF controller

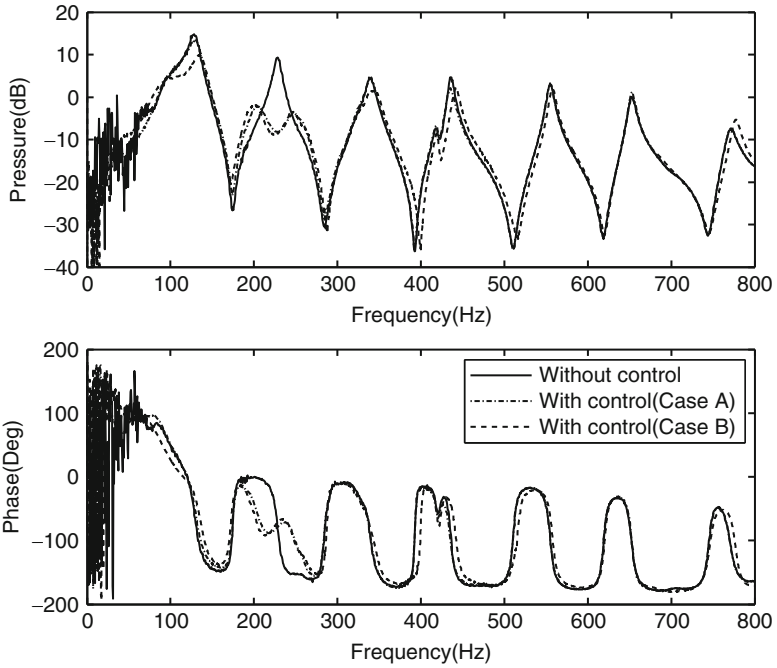

Fig. 6.62 The control performance for rigid duct

References

1. Clark RL, Saunders WR, Gibbs GP (1998) Adaptive structures: dynamics and control. Wiley, New York
2. Moheimani SOR, Fleming AJ (2006) Piezoelectric transducers for vibration control and damping. Springer, Berlin
3. Fanson JL, Caughey TK (1990) Positive position feedback control for large space structures. AIAA J 28(4):717–724
4. Friswell MI, Inman DJ (1999) The relationship between positive position feedback and output feedback controllers. Smart Mater Struct 8:285–291
5. Poh S, Baz A (1990) Active control of a flexible structure using a modal positive position feedback controller. J Intell Mater Syst Struct 1:273–288
6. Hegewald T, Inman DJ (2001) Vibration suppression via smart structures across a temperature range. J Intell Mater Syst Struct 12:191–203
7. Rew KH, Han JH, Lee I (2002) Multi-modal vibration control using adaptive positive position feedback. J Intell Mater Syst Struct 13:13–22
8. Denoyer KK, Kwak MK (1996) Dynamic modelling and vibration suppression of a slewing structure utilizing piezoelectric sensors and actuators. J Sound Vib 189:13–31
9. Moheimani SOR, Vautier BJG, Bhikkaji B (2006) Experimental implementation of extended multivariable ppf control on an active structure. IEEE Trans Control Syst Technol 14(3):443–445
10. Kwak MK, Heo S (2007) Active vibration control of smart grid structure by multiinput and multioutput positive position feedback controller. J Sound Vib 304:230–245
11. Shan J, Liu HT, Sun D (2005) Slewing and vibration control of a single-link flexible manipulator by positive position feedback (PPF). Mechatronics 15(4):487–503
12. Gu H, Song G (2005) Active vibration suppression of a composite I-beam using fuzzy positive position control. Smart Mater Struct 14(4):540–547
13. Nelson PA, Elliott SJ (1992) Active control of sound. Academic, London
14. UAF 42 Universal active filter. http://focus.ti.com/docs/prod/folders/print/uaf42.html

Problems

P.6.1 Consider a SDOF system with PPF controller K, as shown in Fig. 6.6. The controller natural frequency ω_f is set to be the same as the natural frequency of the structure ω_s. Design a MATLAB GUI program to display the control performance and Nyquist diagram with different gain and damping ratio of the controller.

P.6.2 Consider a simply supported uniform beam with a collocated point force actuator and displacement sensor. The beam has an elastic modulus of 10^9 N/m^2, a density of 2,700 kg/m^3 and a thickness of 4 mm. The dimensions of the beam are 0.05 m $\times$ 0.6 m.

(a) Design the optimal parameters for PPF controller to control the second structural mode of the beam. Assume that the collocated actuator/sensor pair is located at $x_s = 0.1$ m.

(b) Check the stability of the control system.

P.6.3 Reconsider Problem 6.2, if the actuator and sensor is non-collocated, such as actuator is located at $x_a = 0.15$ m and the sensor is located at $x_s = 0.35$ m.

(a) Design an optimal all-pass filter for phase compensation as discussed in Sect. 6.3.
(b) Calculate the control performance of the second-order PPF controller with and without all-pass filter.
(c) Compare the control performance for the different order of PPF controller with optimal all-pass filter.